The University of Sydney

School of Civil Engineering
Sydney NSW 2006
AUSTRALIA

http://www.civil.usyd.edu.au/

Centre for Advanced Structural Engineering

Compression Capacity of Hollow Flange Channel Stub Columns

Research Report No R875

Yi Zhu BE
Tim Wilkinson BSc BE MA PhD

February 2007

ISSN 1833-2781

The University of Sydney

School of Civil Engineering
Centre for Advanced Structural Engineering
http://www.civil.usyd.edu.au/

Compression Capacity of Hollow Flange Channel Stub Columns

Research Report No R875

Yi Zhu, BE
Tim Wilkinson, BSc, BE, MA, PhD

February 2007

Abstract:

This paper presents an investigation into the strength of stub columns of hollow flange channel (LiteSteel Beam) sections manufactured by Smorgon Steel Tube Mills. Compression tests on stub columns were performed on a range of 13 groups of specimens. A reliability analysis was undertaken on the test results with respect to the calculation methods of AS/NZS 4600. It was found that the current method of applying the lower web yield stress in the entire section is conservative. Applying the separate flange and web yield stress to the individual components produces higher capacities by approximately 15%, within an acceptable level of reliability. Finite element analyses were carried out to compare the results of numerical simulation with test results and demonstrated a close prediction of the test ultimate load despite some discrepancies were observed.

Keywords:

Hollow flange channel; Local buckling; Cold-formed steel; AS/NZS 4600; Design rules; Finite element analysis

Copyright Notice

School of Civil Engineering, Research Report R875
Compression Capacity of Hollow Flange Channel Stub Columns

y.zhu@civil.usyd.edu.au
wilko@civil.usyd.edu.au

ISSN 1833-2781

Published by:
School of Civil Engineering
The University of Sydney
Sydney NSW 2006
AUSTRALIA

February 2007

This report and other Research Reports published by The School of Civil Engineering are available on the Internet:

http://www.civil.usyd.edu.au

CONTENTS

1 Introduction

1.1 General

Smorgon Steel Tube Mills have used their patented dual welding technology to manufacture a new section - the Hollow Flange Channel (HFC) as shown in Figure 1. This section is being marketed as the LSB, or LiteSteel Beam.

Hollow flange sections are designed to take advantage of properties of hot-rolled sections – in which area is concentrated away from the neutral axis, and the torsional stiffness of hollow sections.

In the mid 1990s, a slightly different cross-sectional shape was manufactured – the Hollow Flange Beam (HFB). The HFB had some unique failure modes such as flexural distortional buckling and bearing failure. Research was required to investigate these failure modes before these sections could be used efficiently and safely. This research included analytical, experimental and numerical studies (Hancock et al (1994), Sully et al (1994), Pi and Trahair (1997), Avery et al (2000)).

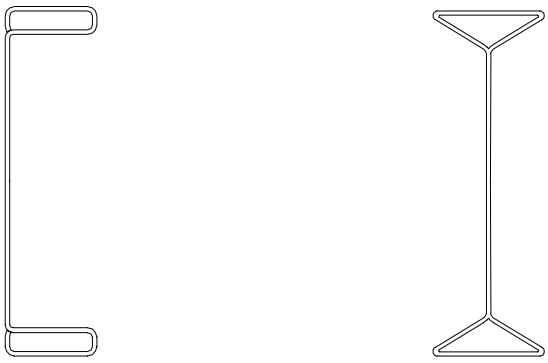

Hollow flange channel Hollow flange beam

Figure 1. Cross-Sectional Shapes

1.2 Behavioural issues

During the cold-forming process, the flat web receives very little additional cold work, compared to the flanges. As a result the nominal yield stress of the flange is f_{yf} = 450 MPa, while for the web it is f_{yw} = 380 MPa.

Compression design for sections with unequal yield stresses is potentially complicated, since the effective width formulation used in calculations is based on the assumption of reaching the yield stress. Considering a fully effective section, in order for the flanges to reach their yield stress of 450 MPa, the webs will not only experience their own yield stress of 380 MPa, but they will experience additional strain past the yield strain, so that the total strain is 450/E

which is as if it had a yield stress of 450 MPa. This is because all parts of the cross section must have equal strain under axial compression.

Figure 2 illustrates the possible compression behaviour of the flange and the web in compression. It is possible that the web strength will start to reduce with increased strain after it has reached yield but before the flange has reached yield. There is some doubt as to whether it is appropriate to assess the web and flange strengths separately, using their respective yield stresses, and then adding the components together. However, the current method used by Smorgon Steel Tube Mills to calculate the design capacity is applying the web yield stress to the entire section

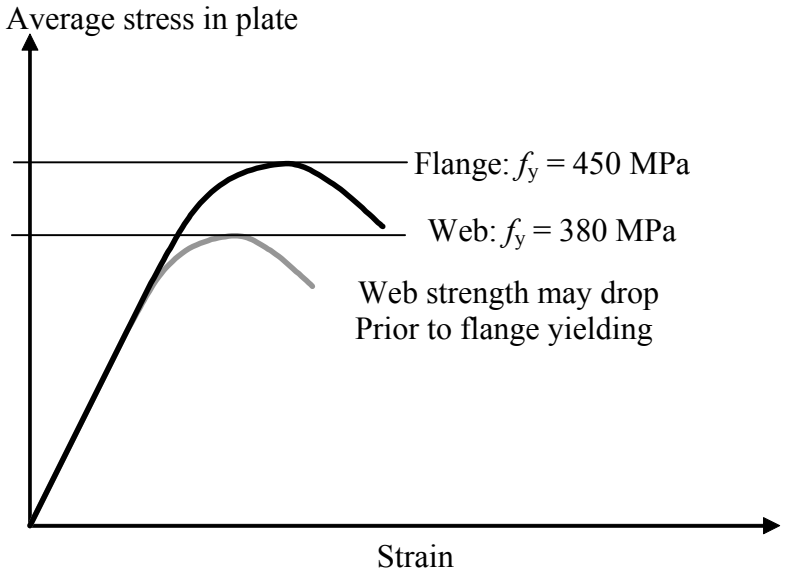

Figure 2. Possible Stress Strain Behaviour in Compression

2 Material Properties

2.1 Coupon test specimens and procedures

The material properties of each series of specimens were determined by tensile coupon tests. At least two longitudinal coupons were tested for each series of specimens. For some specimens of larger cross section dimensions, five longitudinal coupons were fabricated and tested. The coupon dimensions conformed to AS 1391-1991 (Standards Australia, 1991) for the tensile testing of metals. In order to ensure that fracture occurred within the middle portion of the constant gauge length, the test coupons were dimensioned with a more gradual change in cross-section from the constant gauge width to the grip. The width and gauge length of tensile coupons are shown in Figure 3.

The longitudinal coupons were tested according to AS 1391 in the Sintech/MTS 300 kN testing machine. The coupons were tested with the zinc coating

removed. In the tests the longitudinal strains were measured using an extensometer for every coupon, which was attached at the centre of each face.
A data acquisition system was used to record the load and readings of strain during the test.

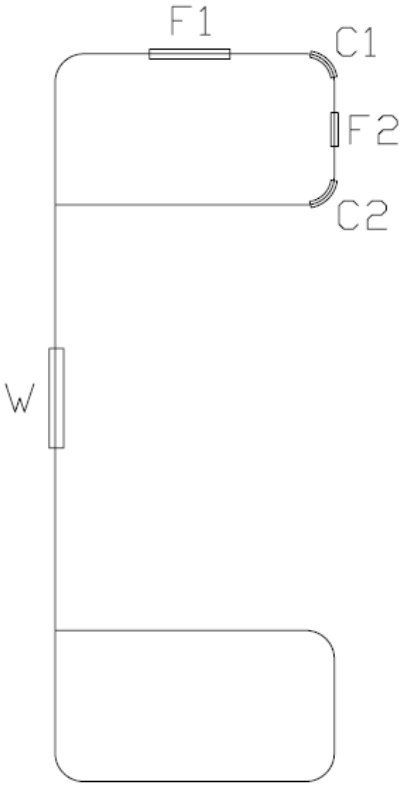

Label of coupons:

300 x 75 x 3.0 x W, F1, F2, C1,C2
300 x 75 x 2.5 x W, F1, F2
300 x 60 x 2.0 x W, F1, F2, C1,C2
250 x 75 x 3.0 x W, F1, F2, C1,C2
250 x 75 x 2.5 x W, F1, F2, C1,C2
250 x 60 x 2.0 x W, F1, F2, C1,C2
200 x 60 x 2.5 x W, F1, C1
200 x 60 x 2.0 x W, F1, C1
200 x 45 x 1.6 x W, F1
150 x 45 x 2.0 x W, F1
150 x 45 x 1.6 x W, F1
125 x 45 x 2.0 x W, F1
125 x 45 x 1.6 x W, F1

Total: 44 coupons

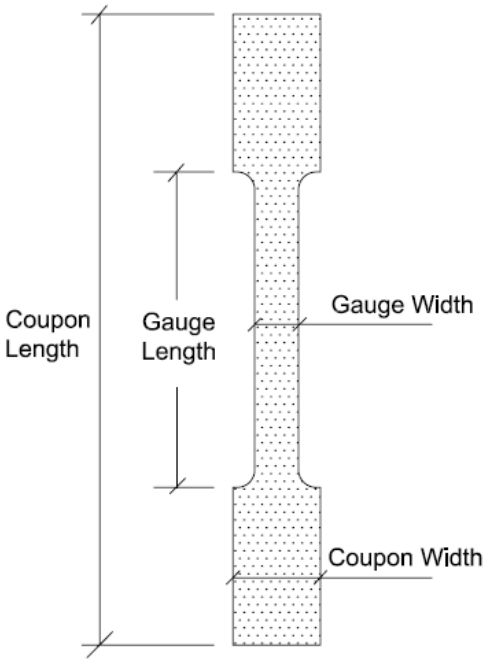

	Coupon width (mm)	Gauge width (mm)	Coupon length (mm)	Gauge length (mm)
Web & Flange 1	25	12.5	180	90
Flange 2	12.5	5	180	90
Corner 1 & 2	10	3	180	90

Figure 3. Dimension of Tensile Coupons

2.2 Coupon test results

The stress-strain curves of specimen 250×60×2.0 LSB obtained from the coupon tests using strain gauges are shown in Figure 4 for coupon of web, flange 1 and corner 1 respectively. Curves for the other specimens are shown in Figure 19 – 30 in the Appendix.

The yield stress f_y was obtained using the nominal 0.2% proof stress. The stress was the measured load divided by the initial cross-section area of the coupon and the strain is the average of the two strain gauge readings. The measured 0.2% proof stress of the steel as well as other material properties are shown for each specimen type in Table 1. Young's modulus of elasticity (E) was also calculated from the elastic part of the stress-strain curves. The calculated mean values of Young's modulus of elasticity were 199 GPa and 212 GPa for web and flange respectively. Percentages of elongation after fracture were also measured and included in Table 1.

From Figure 4 and Table 1, it can be seen that the actual yield stresses of both webs and flanges are higher than the nominal ones. On average, $f_{y,web}/f_{y,web(nominal)} = 1.09$ and $f_{y,flange}/f_{y,flange(nominal)} = 1.28$. Further, the yield stresses of corner coupons as well as flange ones are on average in a similar range, as $f_{y,corner}/f_{y,flange} = 1.02$.

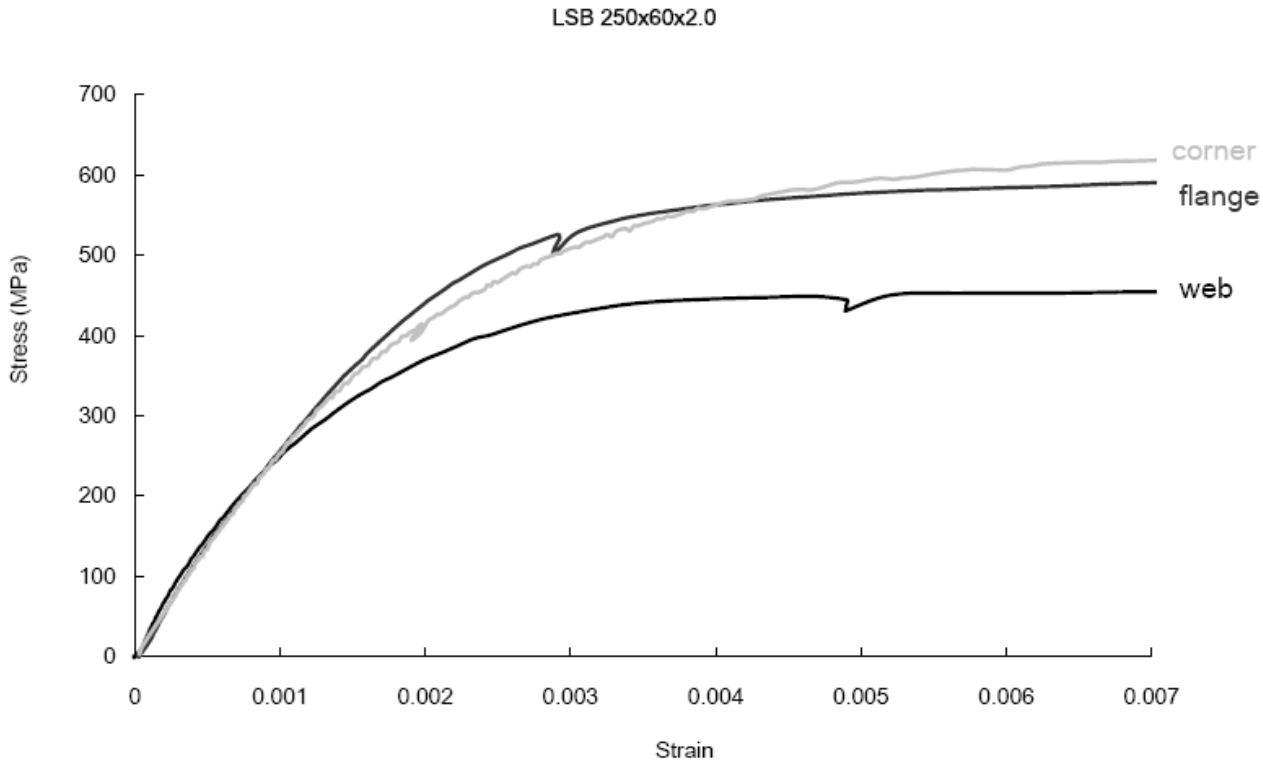

Figure 4. Stress-Strain Curves of Specimen 250×60×2.0 LSB in Web, Flange & Corner from Coupon Test

Designation	web				flange 1				flange 2				corner 1		corner 2	
	f_y (MPa)	f_u (MPa)	E (GPa)	e (%)	f_y (MPa)	f_u (MPa)	E (GPa)	e (%)	f_y (MPa)	f_u (MPa)	E (GPa)	e (%)	f_y (MPa)	f_u (MPa)	f_y (MPa)	f_u (MPa)
300 x 75 x 3.0	430	515	200	40.0	590	640	230	28.9	580	620	185	31.1	600	655	530	585
300 x 75 x 2.5	380	520	200	37.8	545	595	200	28.9	540	600	160	28.9	\	\	\	\
300 x 60 x 2.0	425	500	230	35.6	545	590	180	24.4	585	565	210	26.7	575	650	535	590
250 x 75 x 3.0	375	510	185	40.0	505	590	150	33.3	535	580	200	33.3	605	650	500	560
250 x 75 x 2.5	370	505	170	33.3	530	575	200	28.9	510	555	195	28.9	570	640	530	575
250 x 60 x 2.0	445	525	200	35.6	575	620	220	24.4	570	605	180	26.7	590	645	530	570
200 x 60 x 2.5	345	510	200	28.9	570	630	220	26.7	\	\	\	\	620	680	\	\
200 x 60 x 2.0	395	490	200	35.6	555	595	280	24.4	\	\	\	\	550	595	\	\
200 x 45 x 1.6	445	520	200	33.3	600	640	230	20.0	\	\	\	\	\	\	\	\
150 x 45 x 2.0	430	505	200	35.6	590	630	220	22.2	\	\	\	\	\	\	\	\
150 x 45 x 1.6	450	530	200	28.9	630	685	200	20.0	\	\	\	\	\	\	\	\
125 x 45 x 2.0	430	520	200	31.1	620	665	230	20.0	\	\	\	\	\	\	\	\
125 x 45 x 1.6	465	520	200	31.1	625	680	200	15.6	\	\	\	\	\	\	\	\

Table 1. Actual Material Properties of Specimens from Coupon Tests

3 Stub Column Tests

3.1 Introduction

A stub column is a structural member sufficiently short so as to preclude member buckling when compressed, but sufficiently long to contain the same initial residual stress pattern as a much longer member cut from the same stock. For cold-formed steel sections, which generally have thin-walled plate elements, the stub-column test is aimed at determining the effect of local buckling as well as the effect of cold-forming and residual stress on the section capacity in compression.

3.2 Test Specimens

For cold-formed shapes, the length of the stub column should not be less than three times the largest dimension of the cross section and no more than 20 times the least radius-of-gyration (Galambos, 1988). In the tests in this report, the lengths of stub columns were three times the width. The ends of the columns were milled flat and perpendicular to the longitudinal axis of the column.

Two stub columns in each of the thirteen size ranges were tested. The nominal dimensions are outlined in Figure 5 and Table 2. Measurements of geometry were taken. Regardless of the nominal section sizes, the actual section dimensions were precisely measured and recorded. Table 2 & 3 show the nominal and actual section dimensions of LSB stub column specimens respectively. Thickness is measured at web only.

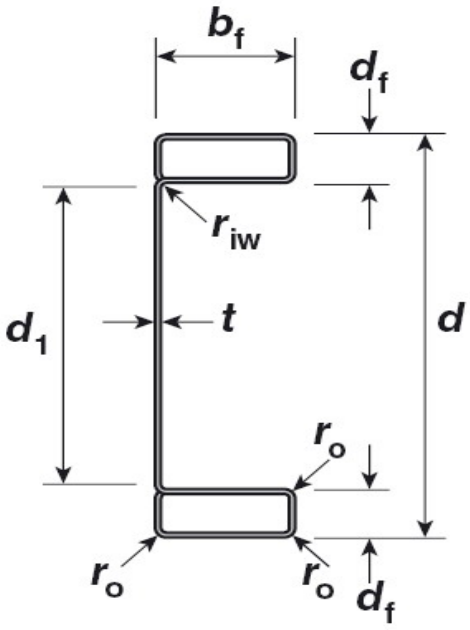

Figure 5. Section Dimension Definitions

Specimen Designation	d	d_f	b_f	t	r_o	r_{iw}	d_1
300×75×3.0 LSB	300	25	75	3.0	6	3	244
300×75×2.5 LSB	300	25	75	2.5	5	3	244
300×60×2.0 LSB	300	20	60	2.0	4	3	254
250×75×3.0 LSB	250	25	75	2.0	6	3	194
250×75×2.5 LSB	250	25	75	2.5	5	3	194
250×60×2.0 LSB	250	20	60	2.0	4	3	204
200×60×2.5 LSB	200	20	60	2.5	5	3	154
200×60×2.0 LSB	200	20	60	2.0	4	3	154
200×45×1.6 LSB	200	15	45	1.6	3.2	3	164
150×45×2.0 LSB	150	15	45	2.0	4	3	114
150×45×1.6 LSB	150	15	45	1.6	3.2	3	114
125×45×2.0 LSB	125	15	45	2.0	4	3	89
125×45×1.6 LSB	125	15	45	1.6	3.2	3	89

Table 2. Nominal Section Dimensions of Specimens (mm)

Specimen Designation	d	d_f	b_f	t	r_o	r_{iw}	d_1
300×75×3.0 LSB (A)	302.5	25.5	75.3	2.88	6.8	3	244
300×75×3.0 LSB (B)	302.3	25.5	75.2	2.87	6.5	3	244
300×75×2.5 LSB (A)	303.8	25.7	75.2	2.51	5.8	3	244
300×75×2.5 LSB (B)	303.8	25.8	75.5	2.51	5.8	3	244
300×60×2.0 LSB (A)	302.3	20.8	59.8	1.95	4.6	3	254
300×60×2.0 LSB (B)	302.3	20.8	59.5	1.94	4.6	3	254
250×75×3.0 LSB (A)	250.3	25.2	75.8	2.82	6.3	3	194
250×75×3.0 LSB (B)	250.3	25.2	75.2	2.81	6.9	3	194
250×75×2.5 LSB (A)	250.3	25.8	75.7	2.50	7.1	3	194
250×75×2.5 LSB (B)	250.3	25.5	75.3	2.50	6.5	3	194
250×60×2.0 LSB (A)	252.3	20.3	59.5	1.93	4.3	3	204
250×60×2.0 LSB (B)	252.0	20.2	59.7	1.94	4.4	3	204
200×60×2.5 LSB (A)	200.8	19.5	60.0	2.51	4.3	3	154
200×60×2.5 LSB (B)	200.8	19.3	60.0	2.52	4.3	3	154
200×60×2.0 LSB (A)	200.0	20.2	59.7	1.93	3.7	3	154
200×60×2.0 LSB (B)	200.0	20.0	60.0	1.93	3.9	3	154
200×45×1.6 LSB (A)	200.8	15.5	44.7	1.60	3.3	3	164
200×45×1.6 LSB (B)	201.0	15.3	44.5	1.59	3.5	3	164
150×45×2.0 LSB (A)	152.5	15.2	45.2	1.97	4.0	3	114
150×45×2.0 LSB (B)	151.3	15.0	45.0	1.96	4.4	3	114
150×45×1.6 LSB (A)	150.0	15.3	44.8	1.59	3.4	3	114
150×45×1.6 LSB (B)	150.0	15.0	44.7	1.58	3.1	3	114
125×45×2.0 LSB (A)	125.8	15.3	44.8	1.92	3.8	3	89
125×45×2.0 LSB (B)	126.0	15.2	45.0	1.92	3.5	3	89
125×45×1.6 LSB (A)	126.0	15.3	45.3	1.56	3.3	3	89
125×45×1.6 LSB (B)	126.0	15.2	44.7	1.55	3.1	3	89

Table 3. Measured Section Dimensions of Specimens (mm)

3.3 Testing

3.3.1 Test set-up

Testing of the 26 LSB stub columns was carried out in a 2000 kN DARTEC hydraulic testing machine. The test arrangement is shown in Figure 6.

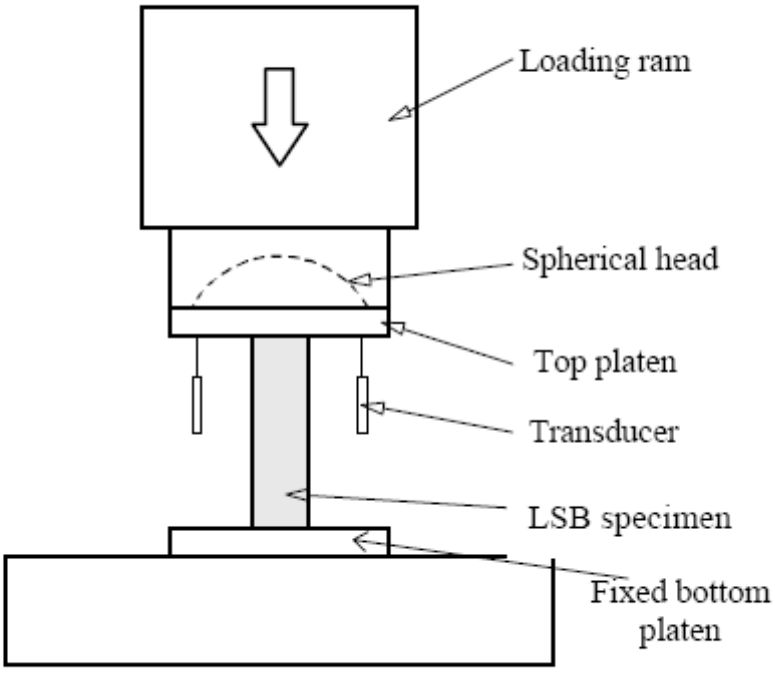

Figure 6. Test Arrangement for Stub Columns

3.3.2 Loading rates

The loading rate for each test was set as 0.9 mm/sec so that ultimate load would be reached after 5-10 minutes, and the test would be completed following an appropriate amount of unloading after 20-25 minutes.

3.3.3 Instrumentation and data acquisition

Three linear variable displacement transducers (LVDTs) were used to determine the end displacement of the stub columns. Seven groups of linear electrical resistance strain gauges were affixed to both surfaces of the webs of some selected specimens at mid-height, in order to investigate the stress-strain behaviour of the web. The strain is the average of the two strain gauge readings. Load, stroke, strain, displacement were all recorded using the data acquisition equipment and the associated computer package.

3.4 Test results

A summary of the results showing the ultimate load for each of the LSB stub column tests is presented in Table 4. The maximum difference between any pair of repeated tests is approximately 9%, and the mean difference is 3.5%. This shows a good level of repeatability.

Designation	Group A (kN)	Group B (kN)
300×75×3.0 LSB	728	735
300×75×2.5 LSB	563	600
300×60×2.0 LSB	356	375
250×75×3.0 LSB	673	651
250×75×2.5 LSB	564	572
250×60×2.0 LSB	369	377
200×60×2.5 LSB	488	489
200×60×2.0 LSB	332	326
200×45×1.6 LSB	248	250
150×45×2.0 LSB	305	310
150×45×1.6 LSB	250	228
125×45×2.0 LSB	314	311
125×45×1.6 LSB	239	217

Table 4. Results from Stub Column Tests

From the measured end displacement readings from the LVDTs and the load recordings from the computer package, the load-end displacement curves from the 26 stub column tests were plotted and some of the typical diagrams are shown in Figures 7 and 8. The other ones are all shown in Figures 31 – 40 in the Appendix.

Local buckling was observed during the tests. The local buckling in the web occurred first and the flange buckled afterwards. This is because the web is much more slender than the flange. Photographs of deformed test specimens are shown in Figure 9.

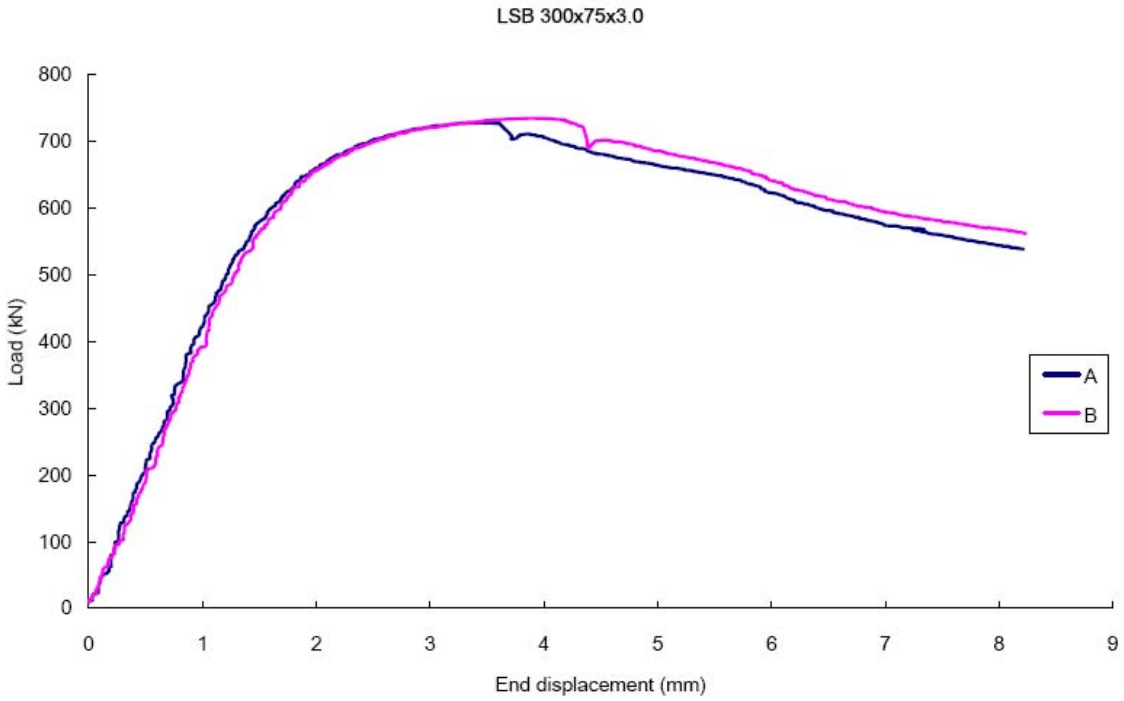

Figure 7. Load - End displacement Curves for 300×75×3.0 LSB Stub Column

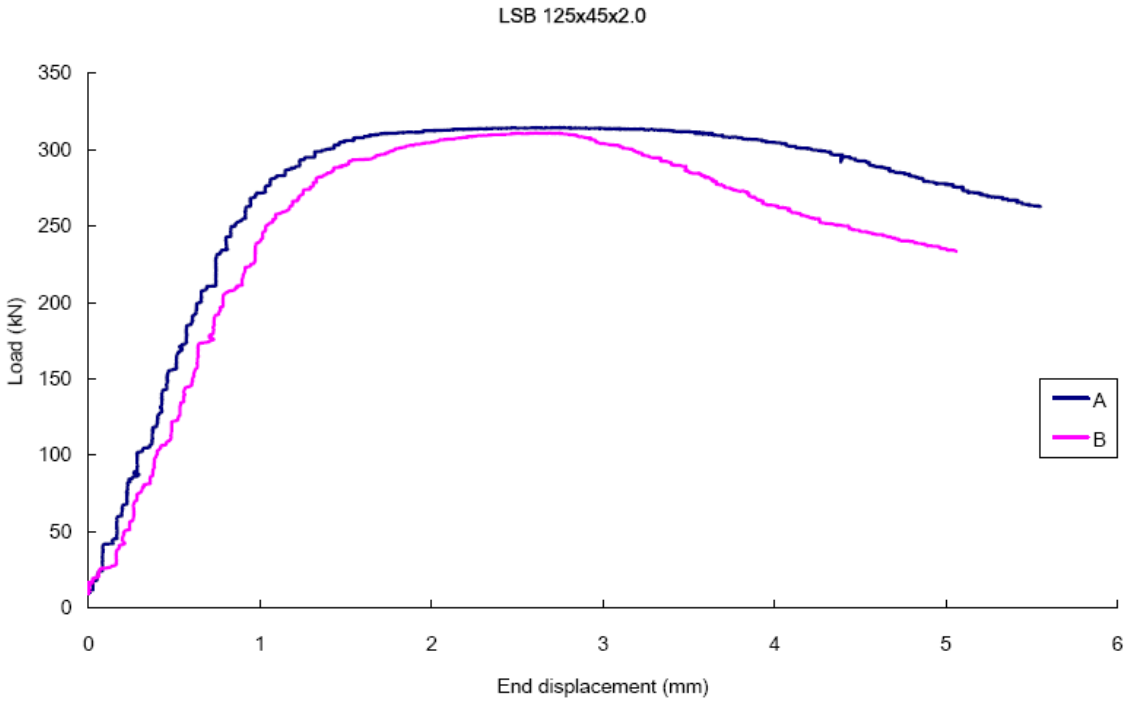

Figure 8. Load - End displacement Curves for 125×45×2.0 LSB Stub Column

Figure 9. Deformation of Tested Specimens
(300×75×2.5 (A) and 150×45×1.6 (A))

4 Test Results and Comparisons with Design Standards

4.1 Comparison of the capacities between test results and calculated results

Since the yield stresses of web and flange are different, there is uncertainty concerning the appropriate method to calculate the capacity. In this paper, four different methods of capacity calculation were attempted and they were compared with the tests results.

The four methods to calculate the capacity are stated as following based on the equation $P = A_e \times f_y$ where f_y refers to the actual yield stress of web or flange:

1) Assume $f_{y,flange}$ for both flange and web through whole calculation.
2) Assume $f_{y,web}$ for both flange and web through whole calculation. This is the current method used in the Design Capacity Tables for LiteSteel Beam (Smorgon Steel, April 2005).
3) Assume $f_{y,flange}$ for flange and $f_{y,web}$ for web through whole calculation.
4) Assume $f_{y,flange}$ for both flange and web when calculating effective section properties. Assume $f_{y,flange}$ for flange and $f_{y,web}$ for web when calculating design capacities.

The key point is to calculate effective section area A_e which can be expressed as $A_e = b_e \times t$. According to Clause 2.2.1.2 of AS/NZS 4600 (2005), effective width (b_e) for capacity calculations shall be determined from Equation 2.2.1.2(1) or Equation 2.2.1.2(2), as appropriate.

For $\lambda \leq 0.673$: $b_e = b$ . . . ...2.2.1.2(1)
For $\lambda > 0.673$: $b_e = \rho b$ . . . 2.2.1.2(2)
where
b = flat width of element excluding radii

ρ = effective width factor = $\dfrac{\left(1-\dfrac{0.22}{\lambda}\right)}{\lambda}$

λ is a slenderness factor determined as follows:

$$\lambda = \sqrt{\frac{f}{F_{cr}}}$$

$$F_{cr} = k\frac{\pi^2 E}{12(1-\mu^2)}\left(\frac{t}{b}\right)^2$$

where
f = design stress in the compression element calculated on the basis of the effective design width. In this report, f is taken equal to actual yield stress on the basis of the effective design width
t = Thickness of the uniformly compressed stiffened elements
μ = Poisson's ratio of steel = 0.3
E = Modulus of elasticity
k = Plate buckling coefficient
= 4 for stiffened elements supported by a web on each longitudinal edge

North American Specification for the Design of Cold-Formed Steel Structural Members (AISI 2001) defines the same effective width method to calculate A_e. Same equations are applied.

The results of group A and B were shown in Table 5. In figures 10 & 11 showing load-displacement curves, dash lines M1, M2, M3 and M4 refer to values of predicted capacities using method 1, 2, 3 and 4, respectively.

Designation	Sample	test result (kN)	M 1 (kN)	P_t/P_{calc}	M 2 (kN)	P_t/P_{calc}	M 3 (kN)	P_t/P_{calc}	M 4 (kN)	P_t/P_{calc}
300×75×3.0	A	728	799	0.91	582	1.25	750	0.97	733	0.99
	B	735	797	0.92	581	1.27	749	0.98	732	1.00
300×75×2.5	A	563	638	0.88	449	1.25	597	0.94	583	0.97
	B	600	639	0.94	450	1.33	598	1.00	584	1.03
300×60×2.0	A	356	391	0.91	310	1.15	374	0.95	367	0.97
	B	375	388	0.97	307	1.22	370	1.01	364	1.03
250×75×3.0	A	673	676	1.00	502	1.34	637	1.06	624	1.08
	B	651	665	0.98	494	1.32	626	1.04	613	1.06
250×75×2.5	A	564	614	0.92	429	1.31	576	0.98	563	1.00
	B	571	615	0.93	429	1.33	576	0.99	563	1.01
250×60×2.0	A	369	398	0.93	317	1.16	380	0.97	373	0.99
	B	377	400	0.94	319	1.18	382	0.99	375	1.01
200×60×2.5	A	488	559	0.87	338	1.44	504	0.97	489	1.00
	B	489	560	0.87	339	1.44	506	0.97	490	1.00
200×60×2.0	A	332	388	0.86	285	1.16	365	0.91	358	0.93
	B	325	387	0.84	285	1.14	365	0.89	357	0.91
200×45×1.6	A	248	272	0.91	203	1.22	258	0.96	252	0.98
	B	250	268	0.93	200	1.25	254	0.98	249	1.00
150×45×2.0	A	305	337	0.91	246	1.24	315	0.97	308	0.99
	B	310	331	0.94	241	1.29	309	1.00	302	1.03
150×45×1.6	A	250	278	0.90	201	1.24	262	0.95	256	0.98
	B	228	274	0.83	200	1.14	258	0.88	253	0.90
125×45×2.0	A	314	339	0.93	235	1.34	316	0.99	309	1.02
	B	311	342	0.91	237	1.31	319	0.97	312	1.00
125×45×1.6	A	239	267	0.90	203	1.18	254	0.94	249	0.96
	B	216	263	0.82	200	1.08	250	0.86	246	0.88
Mean value				0.91		1.25		0.97		0.99
Standard deviation				0.042		0.091		0.044		0.046

Table 5. Comparison of Load Capacities
(M1, M2, M3, M4 refer to Method 1), 2), 3), 4) respectively.)

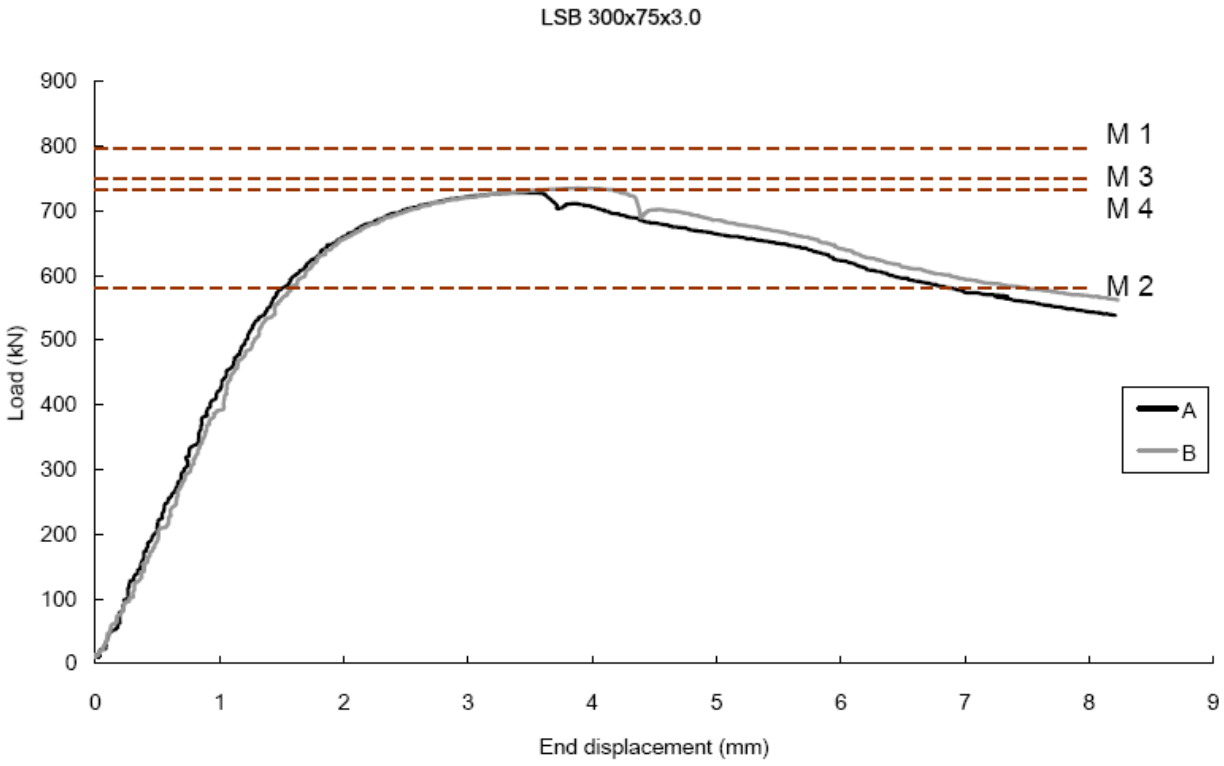

Figure 10. Comparison between Test Results and Four Predicted Methods for 300×75×3.0 LSB Stub Column

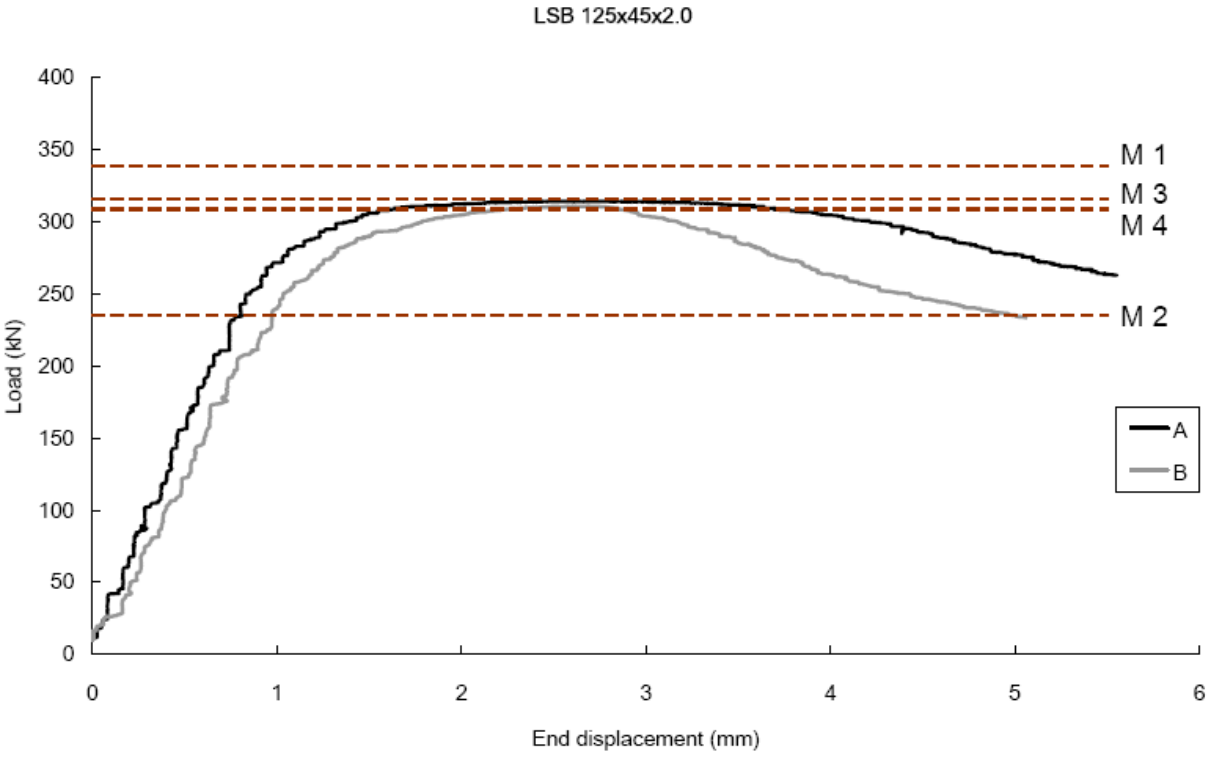

Figure 11. Comparison between Test Results and Four Predicted Methods for 125×45×2.0 LSB Stub Column

4.2 Reliability analysis

Reliability analysis was performed in this paper, based on the First Order Second Moment (FOSM) method described by Ravindra & Galambos (1978). The method assumes a log-normal distribution for the resistance R and the load Q, so that the safety index β is computed from

$$\beta = \frac{\ln\left(R_m/Q_m\right)}{\sqrt{V_R^{\,2} + V_Q^{\,2}}} \tag{I.1}$$

in which R_m is the mean resistance, Q_m is the mean load, V_R is the coefficient of variation of the resistance R, and V_Q is the coefficient of variation of the load Q.

The ratio of the mean resistance R_m to the mean load Q_m may be computed from (Zhao & Hancock 1993)

$$\frac{R_m}{Q_m} = \frac{\gamma_D (D_n / L_n) + \gamma_L}{(D_m / D_n)(D_n / L_n) + (L_m / L_n)} \frac{R_m}{R_n} \frac{1}{\phi} \tag{I.2}$$

in which γ_D is the dead load factor, D_n is the nominal dead load, L_n is the nominal live load, γ_L is the live load factor, D_m is the mean dead load, L_m is the mean live load, R_n is the nominal resistance, and φ is the capacity factor applied to the nominal resistance. According to AS/NZS 4600 (2005), φ is equal to 0.85 for compression members. The ratio of the mean resistance to the mean load, R_m/Q_m, is computed as a function of the ratio D_n/L_n, so all other quantities in Equation (I.2) are constant for a particular type of member.

In accordance with AS/NZS 4600 (2005), the dead load factor γ_D used in the analysis is equal to 1.20, and the live load factor γ_L is equal to 1.50. The ratios D_m/D_n and L_m/L_n are quoted from Ellingwood et al. (1980), which are 1.05 and 1.00, respectively. The ratio R_m/R_n is equal to

$$\frac{R_m}{R_n} = M_m F_m P_m \tag{I.3}$$

in which M_m is the mean ratio of the actual material strength to the nominal material strength, F_m is the mean ratio of the actual geometric property to the nominal geometric property, and P_m is the mean ratio of the ultimate test loads P_t to the predicted failure loads P_p.

The coefficient of variation V_R shown in Equation (I.1) is

$$V_R = \sqrt{V_M^{\,2} + V_F^{\,2} + V_P^{\,2}} \tag{I.4}$$

in which V_P is the coefficient of variation corresponding to P_m, computed for each type of connection from the ratios of ultimate test loads to predicted failure loads.

The coefficient of variation V_Q shown in Equation (I.1) is computed from

$$V_Q = \frac{\sqrt{(D_m / D_n)^2 V_D{}^2 (D_n / L_n)^2 + (L_m / L_n)^2 V_L{}^2}}{(D_m / D_n)(D_n / L_n) + (L_m / L_n)} \qquad \text{(I.5)}$$

in which the coefficients of variation in the dead load V_D and in the live load V_L are 0.10 and 0.25, respectively (Ellingwood et al. 1980). As with the ratio of the mean resistance to the mean load, R_m/Q_m, the coefficient of variation V_Q is computed as a function of the ratio D_n/L_n.

The safety indices β of a particular type of member can therefore be computed for cases ranging from "dead load only" to "live load only". A "live load only" case corresponds to a zero value of D_n/L_n, and a "dead load only" case corresponds to an infinite value of D_n/L_n. The latter case does not present a mathematical difficulty in computing the safety index as a very large value of D_n/L_n (say, 104) can be used with little loss in numerical accuracy. However, the safety indices are normally plotted against $D_n/(D_n+L_n)$, which range from zero for the "live load only" case to unity for the "dead load only" case.

The statistical parameters required for the computation of the safety indices for the LSB specimens using four methods to calculate the design capacity are given in Table 6. The data related to material properties (M_m & V_m) and geometry (F_m & V_F) were obtained from long term tests from Smorgon Steel Tube Mills. It was found that the safety indices vary between 2.714 and 3.930 for method 3, and between 2.795 and 4.085 for method 4. For most loading combinations of these two methods, the safety indices β are within a proper range greater than the target index of 2.5 recommended for members in cold-formed steel structures (AS/NZS 4600), as plotted in Fig. 12. However, the safety indices for method 2 vary between 3.608 and 5.389, which are far greater than 2.5 while some safety indices for method 1 are less than the target index. The variable D_n denotes the nominal dead load, and the variable L_n denotes the nominal live load. Thus the lower bound values correspond to the case of live load only.

	M1	M2	M3	M4
M_m	1.171	1.171	1.171	1.171
V_M	0.058	0.058	0.058	0.058
F_m	1.030	1.030	1.030	1.030
V_F	0.054	0.054	0.054	0.054
P_m	0.909	1.254	0.967	0.989
V_P	0.047	0.073	0.046	0.046
R_m/R_n	1.097	1.513	1.167	1.193
V_R	0.092	0.108	0.092	0.092
β_{min}	2.478	3.608	2.714	2.795
β_{max}	3.466	5.389	3.930	4.085

Table 6. Statistical Parameters of LSB Stub Column Specimens

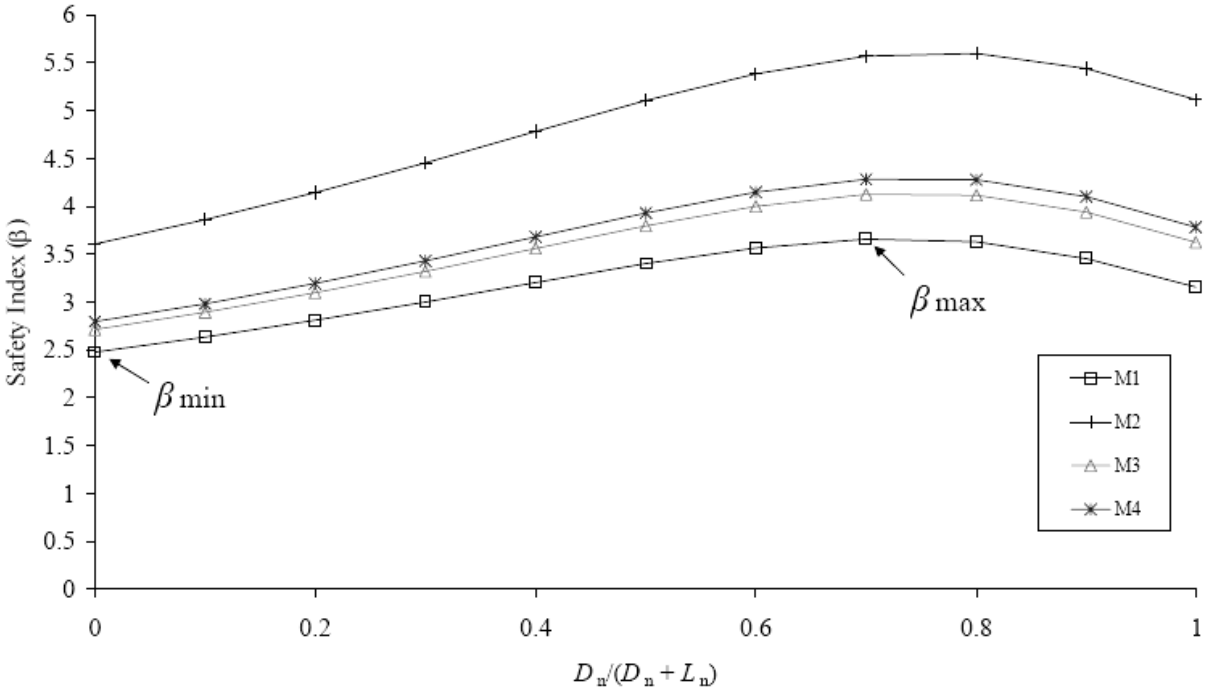

Figure 12. Comparison of Variation of Safety Indices Using Four Methods with Loading Combinations

4.3 Discussion

It was expected that method 1 (β_{min} = 2.478) would not be acceptably reliable since the higher flange yield stress is applied to all parts of the section and

hence it would be overestimating the web strength. Similarly, Method 2 (β_{min} = 3.608) applied the lower web yield stress to the entire section, which is overly conservative.

Method 3 and 4 are only marginally different. The two methods create slightly different effective width in the web, resulting in method 4 being slightly more conservative. Moreover, M4 is more complicated than M3, hence Method 3 (β_{min} = 2.714) is preferably recommended to replace the current method in calculating the design capacities of LSB stub columns. On average, the method 3 capacity predictions using the actual yield stresses are approximately 30% higher than the current method 2 predictions. This is because the measured flange yield stresses are proportionally higher than the nominal ones compared to the web yield stresses. When using nominal yield stresses (f_{yw} = 380 MPa, f_{yf} = 450 MPa), method 3 gives capacities about 15% higher than method 2.

The data of M_m and F_m in Table 6 were obtained from long term LSB tensile test data from Smorgon Steel Tube Mills. It is unusual for the mean ratio F_m to be greater than one. The precision of modern manufacturing processes means that steel makers will aim to produce products at the lower end of the tolerances permitted in design standards, and hence measured geometric properties are nearly always lower than nominal. However, in the absence of other data to the contrary, it suggested the current value should be used, but it is highly recommended that the reliability analysis be repeated when more data related to M_m and F_m is available from Smorgon Steel Tube Mills.

4.4 Design Recommendations

The results show that LSB stub column strength can be obtained by applying the different yield stress of f_{yw} to the web and f_{yf} to the flange. Based on nominal material properties, this will allow for an increase in the sectional capacity in axial compression of approximately 15%. This method of calculation has an acceptable level of reliability and is preferably recommended.

5 Numerical Analysis

5.1 Finite Element Analysis

The finite element analysis program "ABAQUS" was used to simulate the buckling behaviour of LiteSteel stub columns under compression.

5.1.1 Element type

The element type S4R was used in this report. S4R is a general-purpose, finite-membrane-strain, reduced integration shell element. The ratio of length to width of element was about 1:1.

For the whole column, different mesh densities were adopted. In the transverse direction, the finer mesh was used at the flanges based on the concept of effective area. In the longitudinal direction of the column, the mesh density was kept consistent. The mesh density for ABAQUS models of LSB sections is shown in Figure 13.

Figure 13. Mesh of ABAQUS Models of LSB Section

5.1.2 Material behaviour

Most materials of engineering interest initially respond elastically. If the load exceeds some limit, some part of the deformation will remain when the load is removed. Plasticity theories model the material's mechanical response as it undergoes such nonrecoverable deformation in a ductile fashion. Most of the plasticity models in ABAQUS are "incremental" theories in which the mechanical strain rate is decomposed into an elastic part and a plastic part.

The elastic response can be modeled accurately as being linear. The plastic strain values were used for the post buckling analysis. The data for web and flange used in the ABAQUS model was obtained from the stress-strain curves of web and flange from the coupon tests, respectively. The second point on the stress-strain curve corresponded with the onset of plasticity. Typical data used are shown in Table 7.

Web

True Stress (MPa)	Plastic Strain
260	0.00000
279	0.00006
289	0.00011
300	0.00013
333	0.00022
362	0.00038
370	0.00046
404	0.00081
431	0.00201
435	0.00822
440	0.01343
444	0.01608
450	0.01753
481	0.03285
507	0.04706
528	0.06241
547	0.08060
563	0.10069
585	0.13533
600	0.16383

Flange

True stress (MPa)	Plastic strain
392	0.00000
455	0.00008
477	0.00014
503	0.00025
505	0.00035
541	0.00067
574	0.00141
593	0.00226
615	0.00427
626	0.00624
635	0.00881
645	0.01362
657	0.02470
662	0.03185
670	0.04894
680	0.07945

Table 7. Stress-Strain Data Used in ABAQUS for Specimen 300×75×3.0

5.1.3 Boundary condition

For each of the two ends, two different types of boundary conditions were used to simulate the test situation in the column tests. The ends were divided into a fixed end and a movable end. At the fixed end, displacement degrees of freedom in 1, 2, 3 directions (U_1, U_2, U_3) as well as rotational degrees of freedom in 1, 2, 3 directions (θ_1, θ_2, θ_3) were restrained to be zero. At the movable end, load was exerted with an even stress distribution in the longitudinal direction U_3. The simplified representation of boundary conditions is shown in Figure 14.

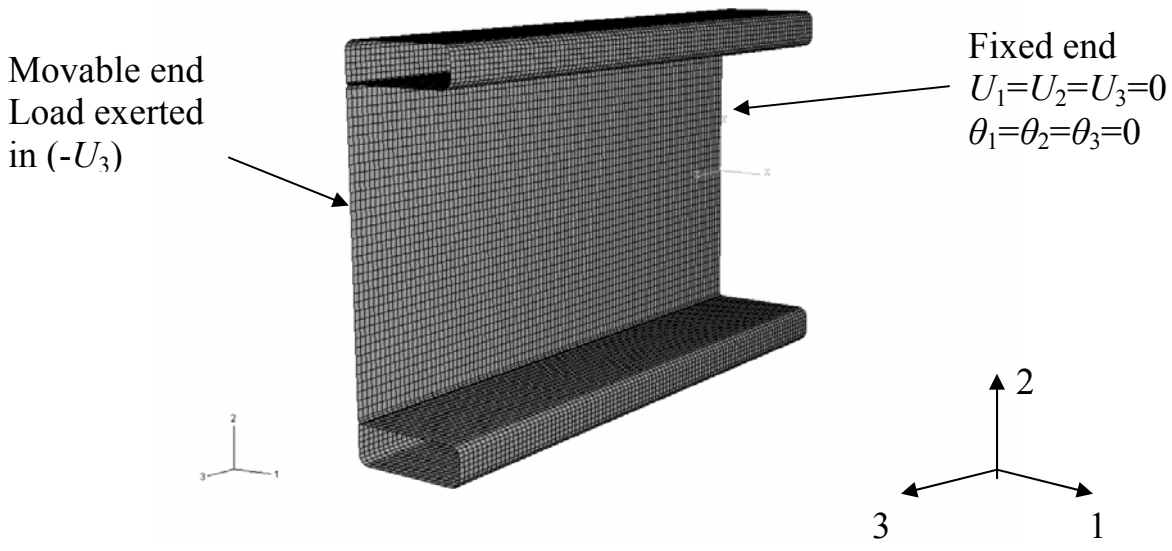

Figure 14. Boundary Conditions for LSB Stub Column in Compression

5.1.4 Geometrical imperfections

To obtain the ultimate loads of the section which undergo buckling, the structure must have initial geometric imperfections to trigger deformation. This can be done by either modelling the structure with an initial out-of-plane deflection or by using small transverse forces (Chou, Chai and Ling, 2000). In this report, the linear buckling mode shape was used to create an initial geometric imperfection for the non-linear post-buckling analysis.

The degree of initial imperfection was specified as the maximum amplitude of the buckling mode shape and was usually prescribed as a percentage of the thickness of sheet steel. Pekoz and Schafer (Pekoz & Schafer, 1996) suggested expression for the average degree of imperfection for the cold-formed steel members is between 0.14t and 0.66t, where t is the thickness of sheet steel. Hence in this study, the results based on the Pekoz's suggested expression were used in finite element analyses. Four grades of geometrical imperfection values were applied which were 0.01t, 0.14t, 0.66t and 1.50t.

5.2 Results

Thirteen specimens of LSB stub columns with different section sizes were set up and their buckling behaviours under axial compression were simulated using ABAQUS. The deformation shapes from ABAQUS analysis were shown in Figure 15 and 16. A series of results mainly of the ultimate loads were obtained.

5.2.1 ABAQUS results

The results of the ultimate loads obtained from ABAQUS were shown in Table 8. Comparing the results between four different imperfection values, the maximum differences were given. From the table, it can be seen that the differences were within 2.50%, which indicates the four results using various imperfection values are of a very close level.

Specimen designation	Ultimate Load from Tests P_{tests} (kN)	ABAQUS Results P_{ABAQUS} (kN)				Maximum Difference between different imperfection values	Maximum Difference between P_{test} and P_{ABAQUS}
		imperfection values					
		0.01t	0.14t	0.66t	1.50t		
300×75×3.0 LSB	728	797	796	801	800	0.62%	8.50%
300×75×2.5 LSB	600	644	641	643	642	0.47%	6.40%
300×60×2.0 LSB	356	390	390	391	393	0.76%	8.72%
250×75×3.0 LSB	673	715	717	719	717	0.56%	6.20%
250×75×2.5 LSB	564	621	619	620	618	0.48%	8.95%
250×60×2.0 LSB	369	408	409	408	408	0.24%	9.70%
200×60×2.5 LSB	488	548	545	547	547	0.55%	10.54%
200×60×2.0 LSB	332	368	367	367	366	0.54%	9.50%
200×45×1.6 LSB	248	269	266	267	268	1.12%	6.60%
150×45×2.0 LSB	305	327	326	327	325	0.61%	6.47%
150×45×1.6 LSB	250	274	277	272	272	1.81%	9.84%
125×45×2.0 LSB	314	331	332	330	332	0.60%	5.38%
125×45×1.6 LSB	239	259	255	261	258	2.30%	6.26%

Table 8. Comparison of Ultimate Loads between ABAQUS Results and Test Results with Various Geometrical Imperfections

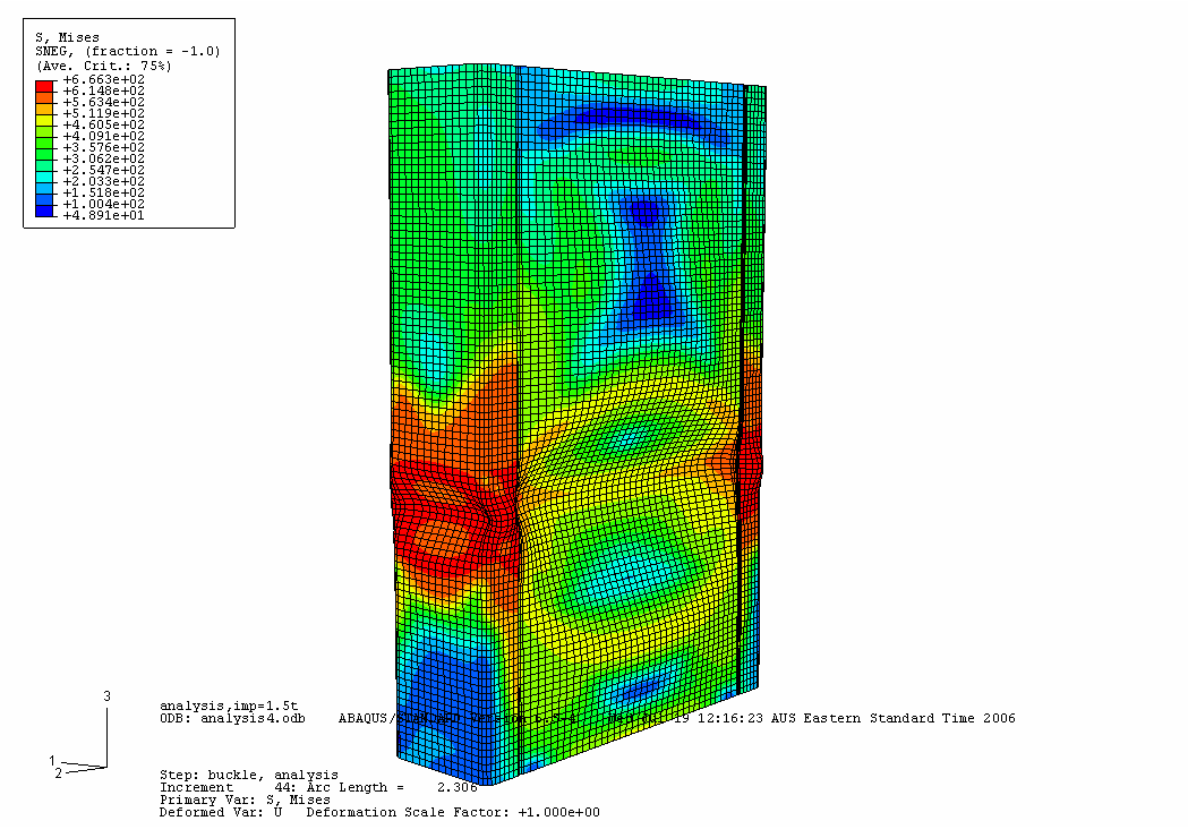

Figure 15. Deformation Shapes of 300×75×3.0 LSB from ABAQUS Results

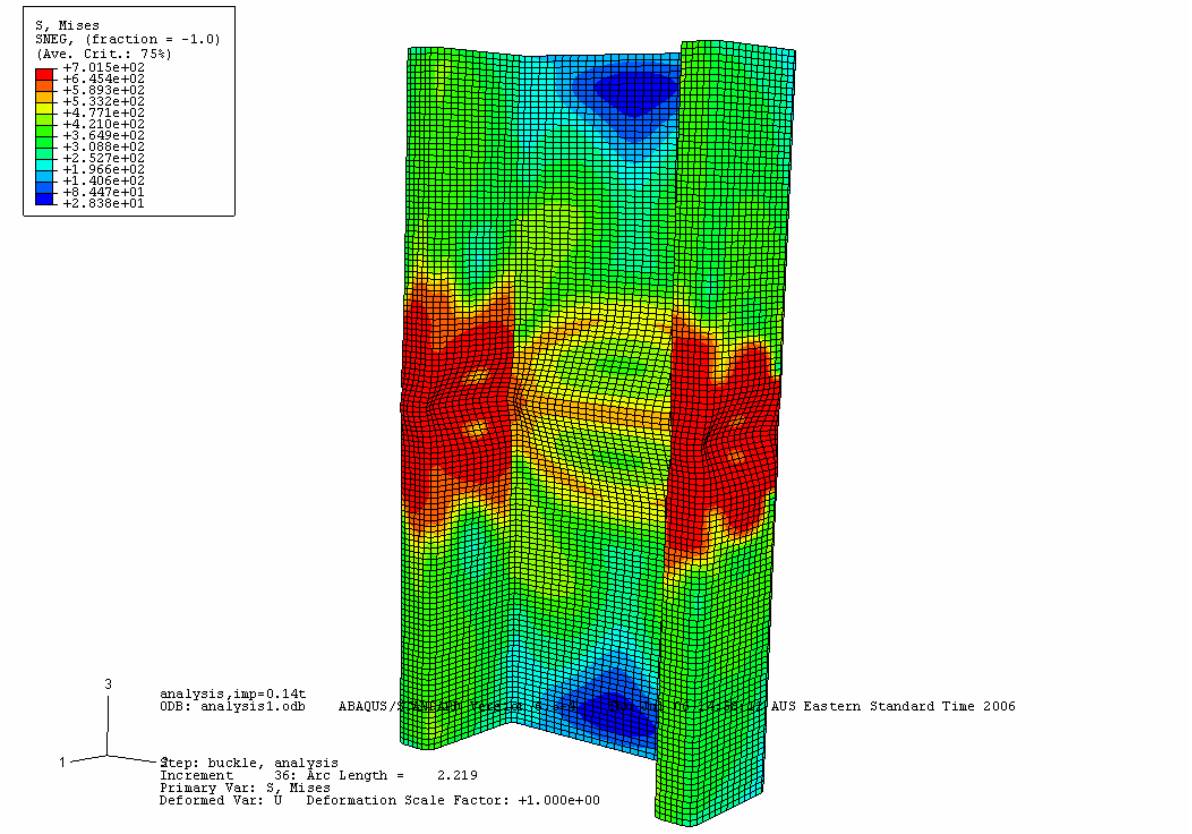

Figure 16. Deformation Shapes of 125×45×1.6 LSB from ABAQUS Results

5.2.2 Comparison between ABAQUS results and test results

The comparison of ultimate loads between ABAQUS results and test results with various geometrical imperfections were also included in Table 10. For four different results of ultimate loads from ABAQUS due to different imperfections, average values were used to be compared with the test results, which provided with the differences between them. The table illustrates that, for all sets of specimens, the ABAQUS results were greater than the test results. The differences vary from 5.38% to 10.54%, fluctuating around 8% on average.

Figure 17 and 18 show the load-displacement curvatures in compression of LSB specimen 200×45×1.6 and 250×60×2.0 from tests and from ABAQUS simulation results.

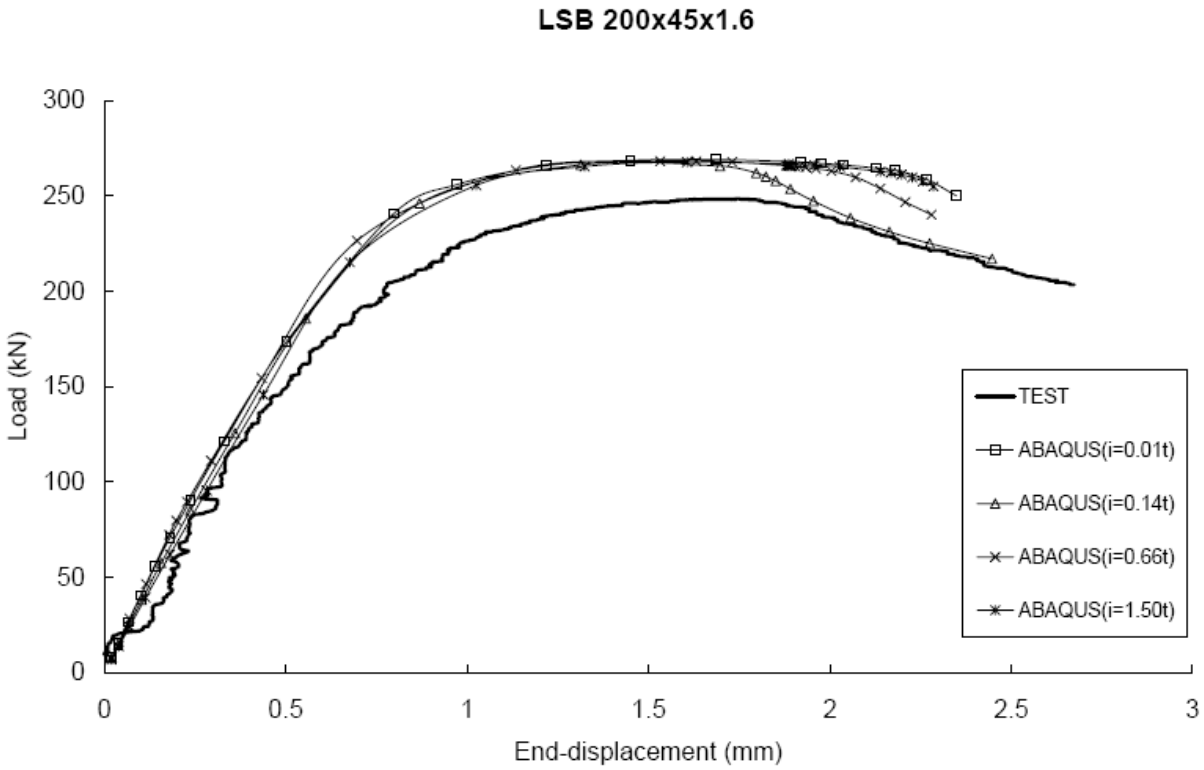

Figure 17. Load-displacement Curvatures of Specimen 200×45×1.6 LSB from Tests and ABAQUS

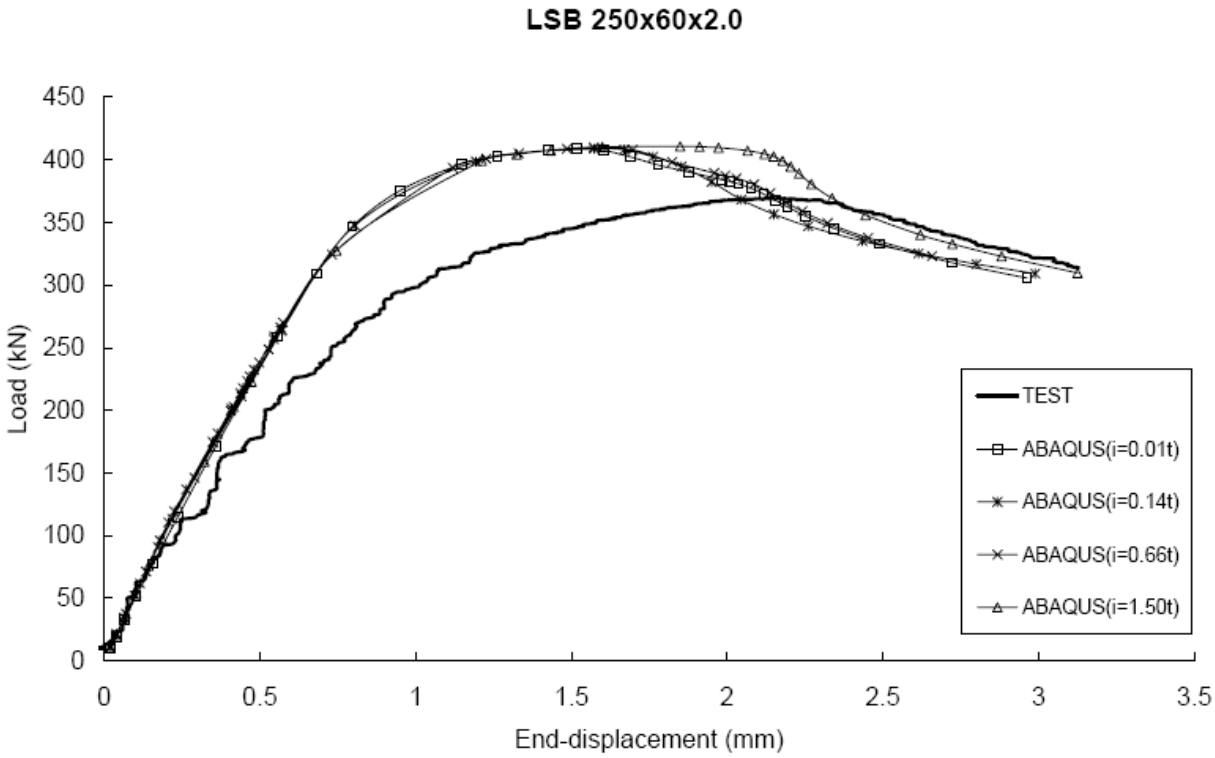

Figure 18. Load-displacement Curvatures of Specimen 250×60×2.0 LSB from Tests and ABAQUS

5.3 Discussion

From Table 8, it can be seen that, in the ABAQUS simulation of the compression tests on LSB specimens, different values of geometrical imperfection did not affect the load capacities significantly. The maximum difference was only 2.30%. This is because the high slenderness of the LSB cross section properties reduces the geometrical imperfection sensitivity in their buckling behaviour.

The comparison between test results and ABAQUS results show that all the ABAQUS results were on average 8% higher than the test results, regardless of various values of geometrical imperfection attempted. The figures plotting the curvatures of both results also illustrate that the ABAQUS results overestimate the real test results. This difference may be mainly due to the residual stresses that existed in the test specimens but not included in the ABAQUS analyses. The residual stresses may have reduced compression capacities of the actual specimens. Another reason for this may be the discrepancy of the material properties input to ABAQUS which did not quite match the real material properties of the specimens. Nevertheless, the test ultimate load can generally be closely predicted numerically.

6 Summary

In this paper, a series of compression tests of hollow flange channel stub columns was carried out, followed by numerical simulation using ABAQUS.

The different yield stresses in the flange and the web make it more complicated to use the effective width approach to determine the stub column strength. The test results were used to apply in the reliability analysis on four different methods in capacity calculation based on the Effective Width Method according to AS/NZS 4600.

The results from reliability analysis show that the current method used by Smorgon Steel is conservative to apply in calculating the compression capacities. The use of the separate flange and web yield stresses in determining the effective width and strength of those elements gives results that have an acceptable level of reliability. This approach should replace the current conservative method of applying the lower web yield stresses to the entire section in calculating the load capacities of LSB stub columns. The capacity prediction using this recommended method is approximately 10-15% higher than the current method.

The ABAQUS results show that the test ultimate load can generally be closely predicted numerically, and is relatively insensitive to geometrical imperfections. The ABAQUS results were on average 8% overestimating the test results due to several reasons.

7 References

American Iron and Steel Institute. "North American Specification for the Design of Cold-Formed Steel Structural Members", Washington DC, USA, 2001.

Standards Australia/Standards New Zealand (1996), Australian/New Zealand Standard AS/NZS 4600 Cold-Formed Steel Structures, Standards Australia/Standards New Zealand, Sydney, Australia.

Standards Australia/Standards New Zealand (1998), Cold-Formed Steel Structures Commentary, Supplement to AS/NZS 4600:1996, Standards Australia/Standards New Zealand, Sydney, Australia.

Standards Australia/Standards New Zealand (2003), Australian/New Zealand Standard Public Draft DR 03518 Cold-Formed Steel Structures, Standards Australia/Standards New Zealand, Sydney, Australia.

Standards Australia/Standards New Zealand (2005), Australian/New Zealand Standard AS/NZS 4600 Cold-Formed Steel Structures, Standards Australia/Standards New Zealand, Sydney, Australia.

Avery, P., Mahendran, M. and Nasir, A., (2000), "Flexural Capacity of Hollow Flange Beams", Journal of Constructional Steel Research, Elsevier, Vol 53, No 2, pp 201-223.

CASE, (1993), "Hollow Flange Beams Under Combined Bending and Bearing", Investigation Report S958, Centre for Advanced Structural Engineering, School of Civil and Mining Engineering, The University of Sydney, Sydney, Australia.

Hancock, G. J., Sully, R. M., and Zhao, X-L., (1994), "Hollow Flange Beams and Rectangular Hollow Sections Under Combined Bending and Bearing", Tubular Structures VI, Proceedings of the 6th International Symposium on Tubular Structures, Melbourne, Australia, Balkema (publ), Grundy, Holgate and Wong (eds.), pp 47 – 54.

Ellingwood, B., Galambos, T. V., MacGregor, J. G., and Cornell, C. A. (1980). Development of a Probability Based Load Criterion for American National Standard A58, National Bureau of Standards, Gaithersburg, Maryland.

Ravindra, M. K., and Galambos, T. V. (1978) "Load and resistance factor design for steel." Journal of the Structural Division, ASCE, 104, 1337-1353.

Chou S.M., Chai G.B and Ling L., "Finite element technique for design of stub columns", Thin-Walled Structures Vol. 37(2), 97-112, 2000.

B.W.Schafer, T.Pekoz, "Computational modelling of cold-formed steel: characterizing geometric imperfections and residual stresses", Journal of Constructional Steel Research 47 (1998), 193-210.

Smorgon Steel LiteSteel Technologies (2005), The Design Capacity Tables for LiteSteel Beam, Smorgon Steel, April 2005.

8 Notation

A	area of the full cross-section
A_e	effective area of the cross-section
B	flat width of element excluding radii
b_f	overall width of a flange
d	overall depth of the section
d_1	depth of the flat portion of a web
d_f	overall depth of a flange
E	Young's modulus of elasticity
e_f	strain over a gauge length of $5.65\sqrt{S}$
f_y	minimum yield stress
f_u	minimum tensile stress
k	plate buckling coefficient
P	point load
r_o	outside bend radius of the flanges
r_{iw}	inside bend radius of the web to flange junction
t	nominal base steel thickness of a section
ρ	effective width factor

9 Appendix

9.1 Stress-strain curves from coupon tests

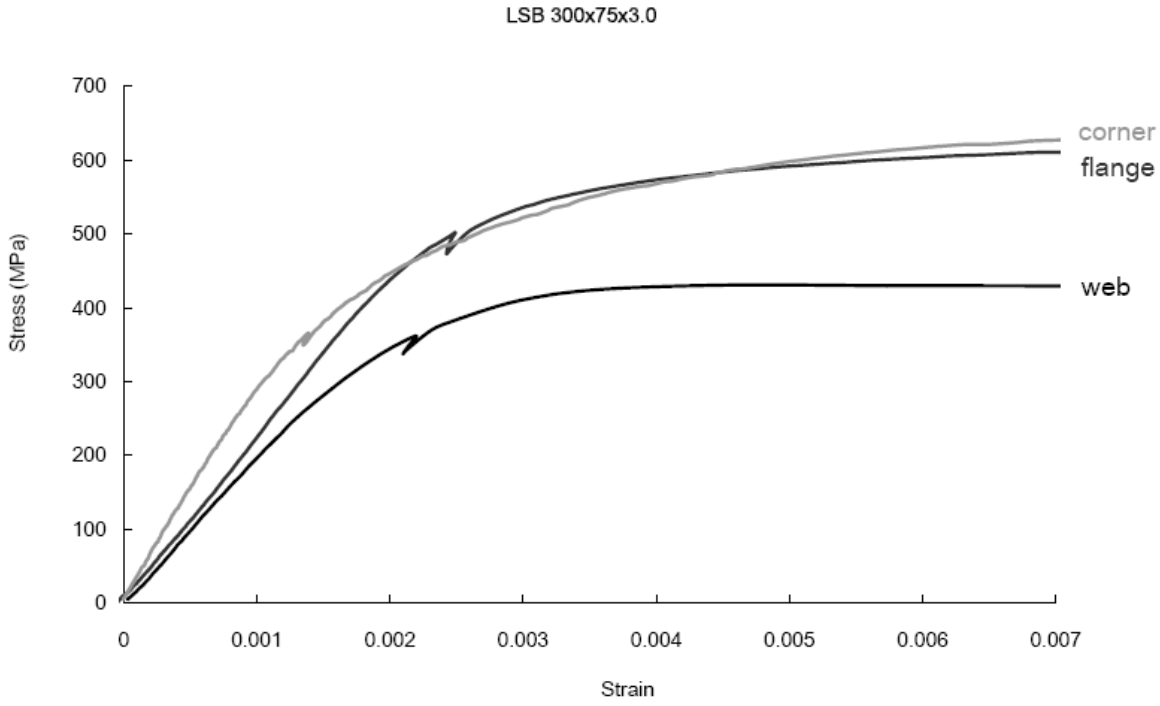

Figure 19. Stress-strain Curves of Specimen 300×75×3.0 in Web, Flange & Corner from Coupon Test

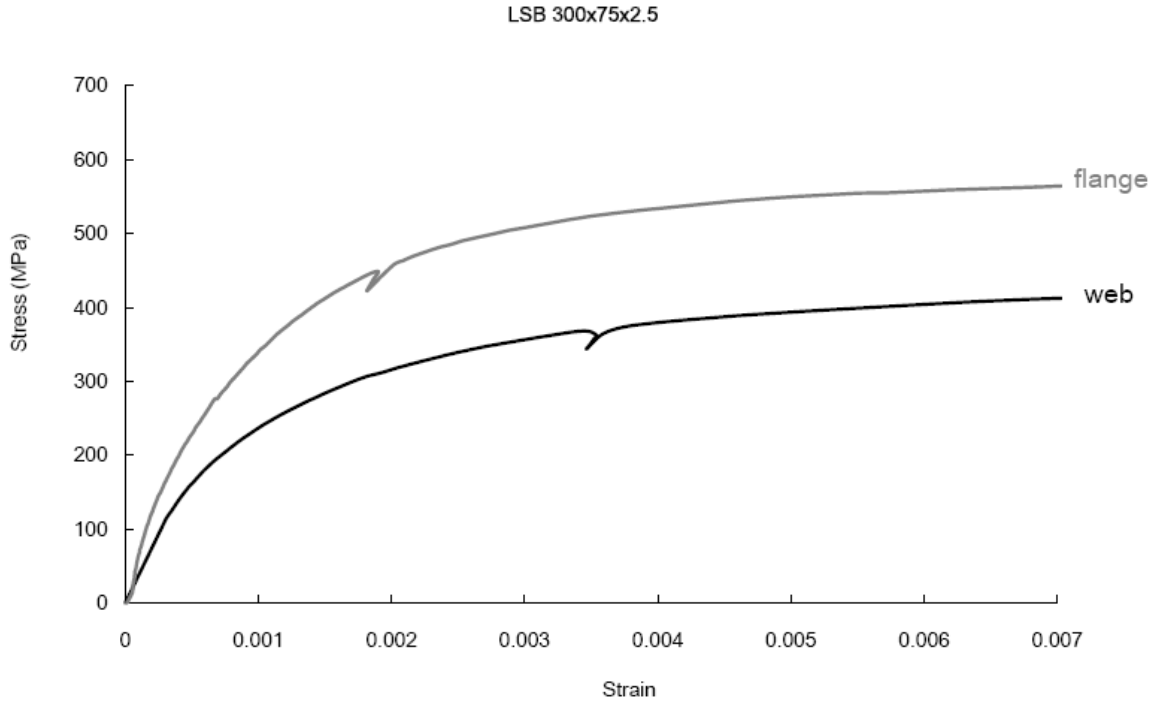

Figure 20. Stress-strain Curves of Specimen 300×75×2.5 in Web, Flange & Corner from Coupon Test

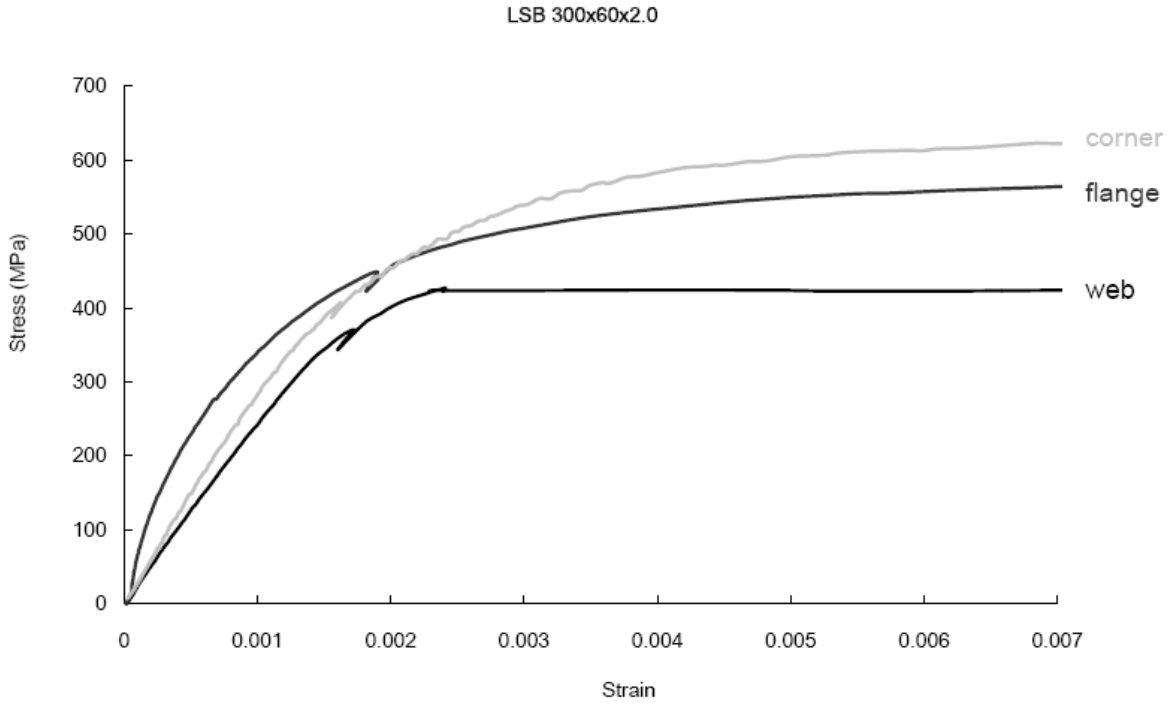

Figure 21. Stress-strain Curves of Specimen 300×60×2.0 in Web, Flange & Corner from Coupon Test

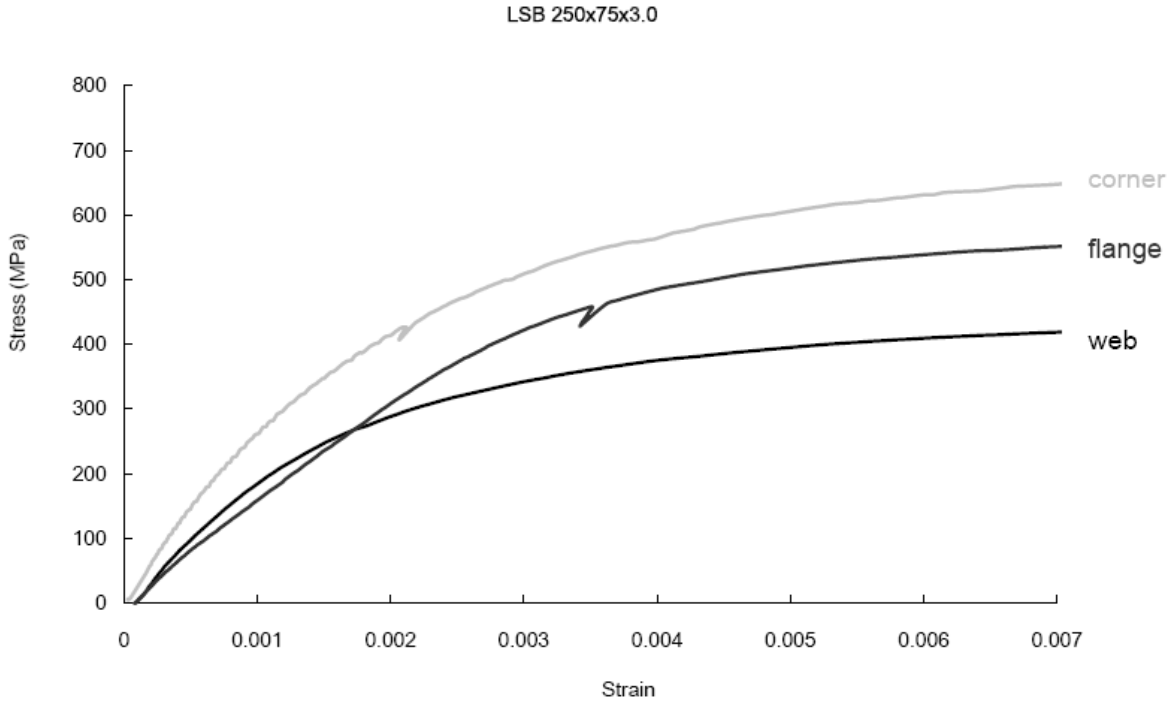

Figure 22. Stress-strain Curves of Specimen 250×75×3.0 in Web, Flange & Corner from Coupon Test

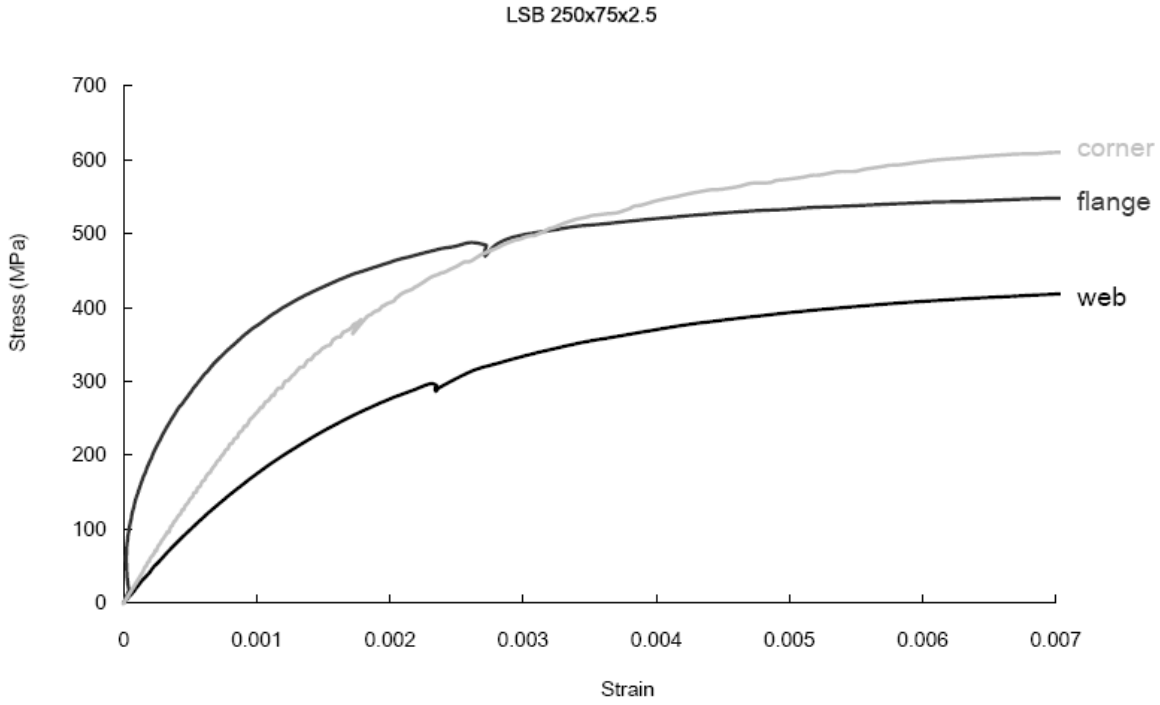

Figure 23. Stress-strain Curves of Specimen 250×75×2.5
in Web, Flange & Corner from Coupon Test

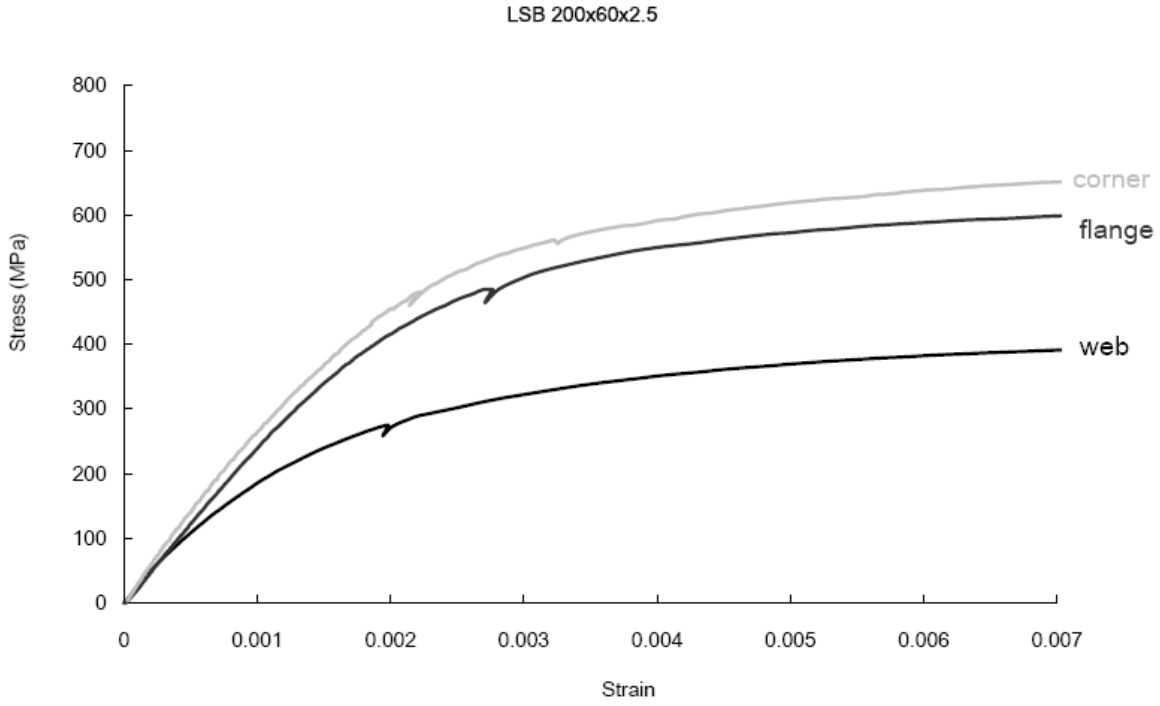

Figure 24. Stress-strain Curves of Specimen 200×60×2.5
in Web, Flange & Corner from Coupon Test

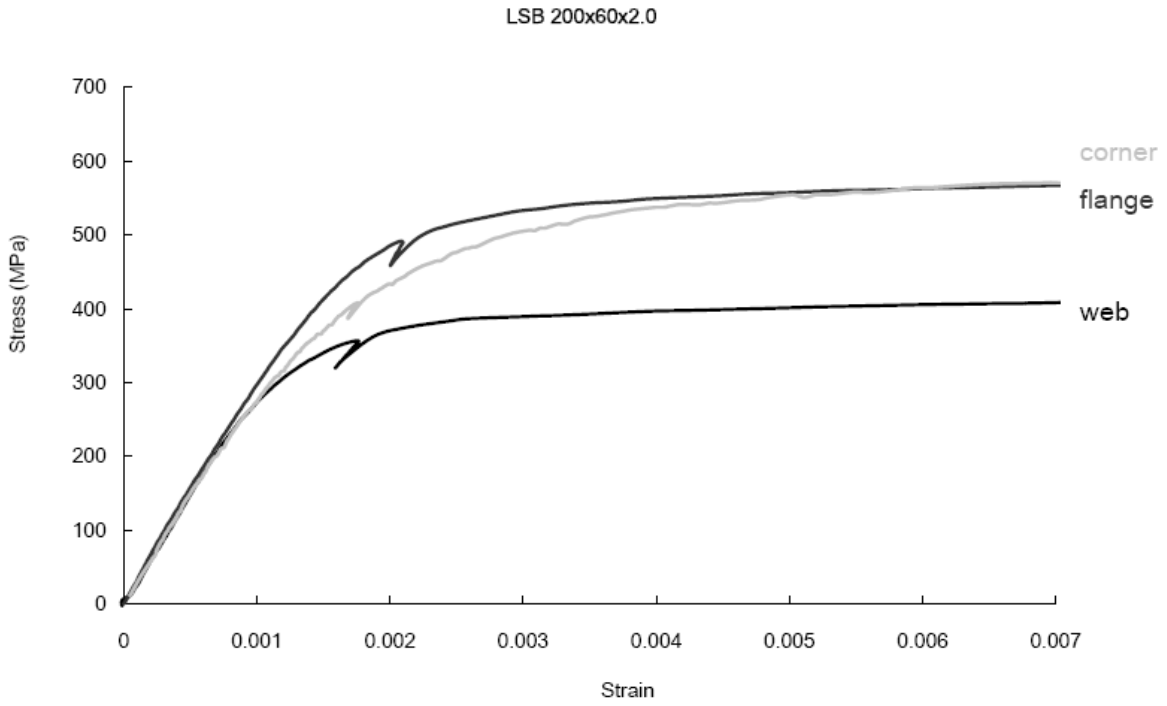

Figure 25. Stress-strain Curves of Specimen 200×60×2.0
in Web, Flange & Corner from Coupon Test

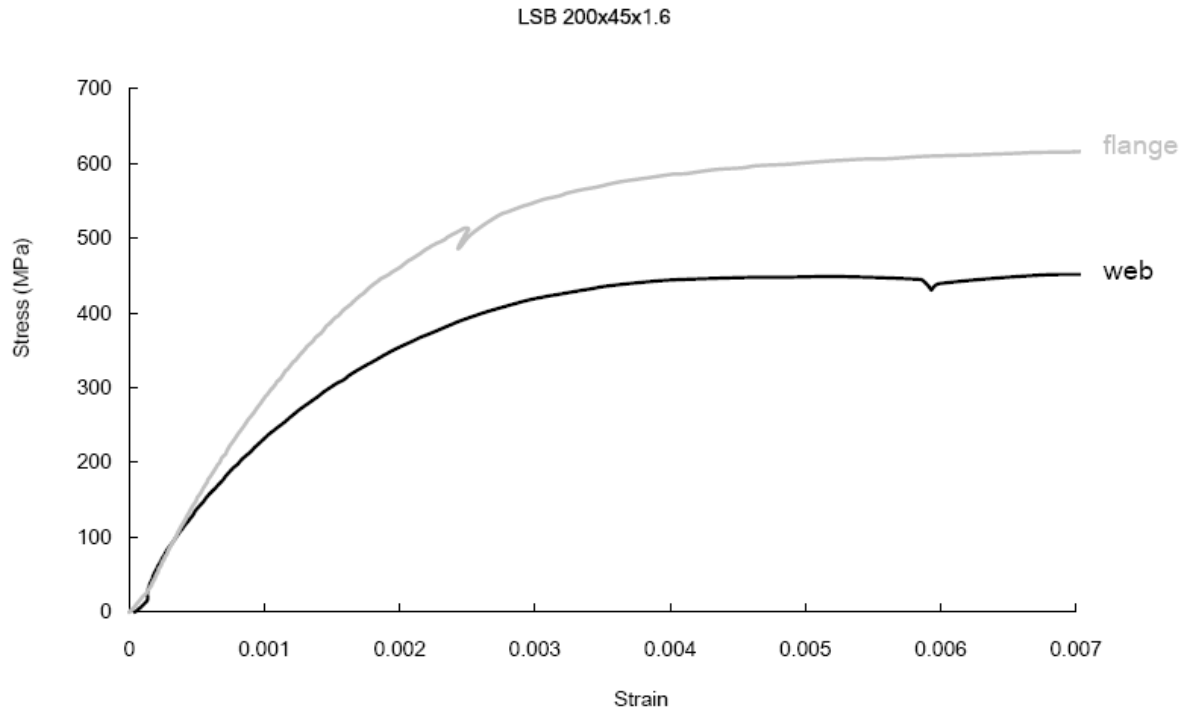

Figure 26. Stress-strain curves of Specimen 200×45×1.6
in Web, Flange & Corner from Coupon Test

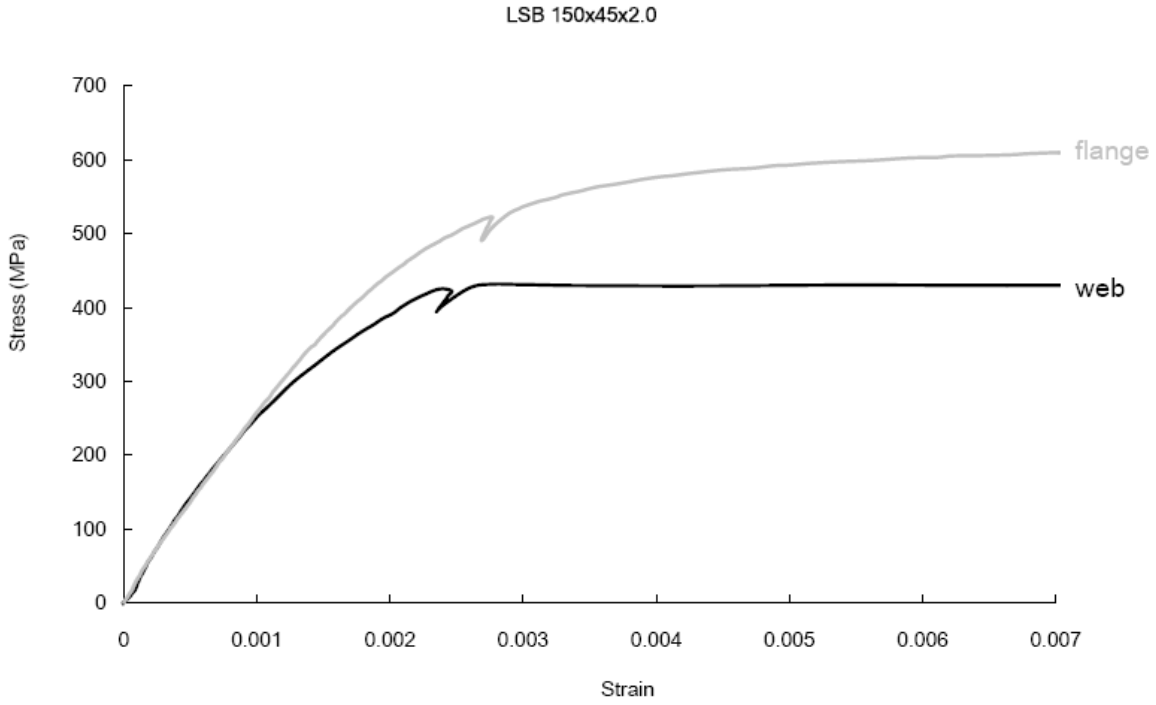

Figure 27. Stress-strain Curves of Specimen 150×45×2.0 in Web, Flange & Corner from Coupon Test

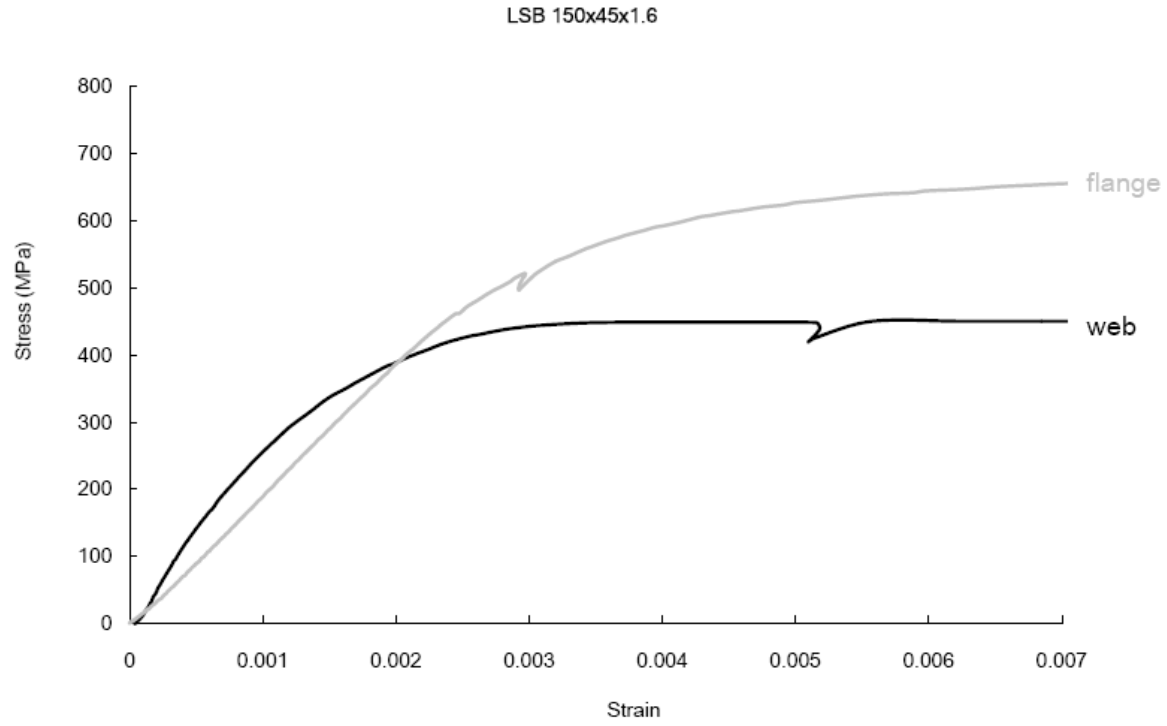

Figure 28. Stress-strain Curves of Specimen 150×45×1.6 in Web, Flange & Corner from Coupon Test

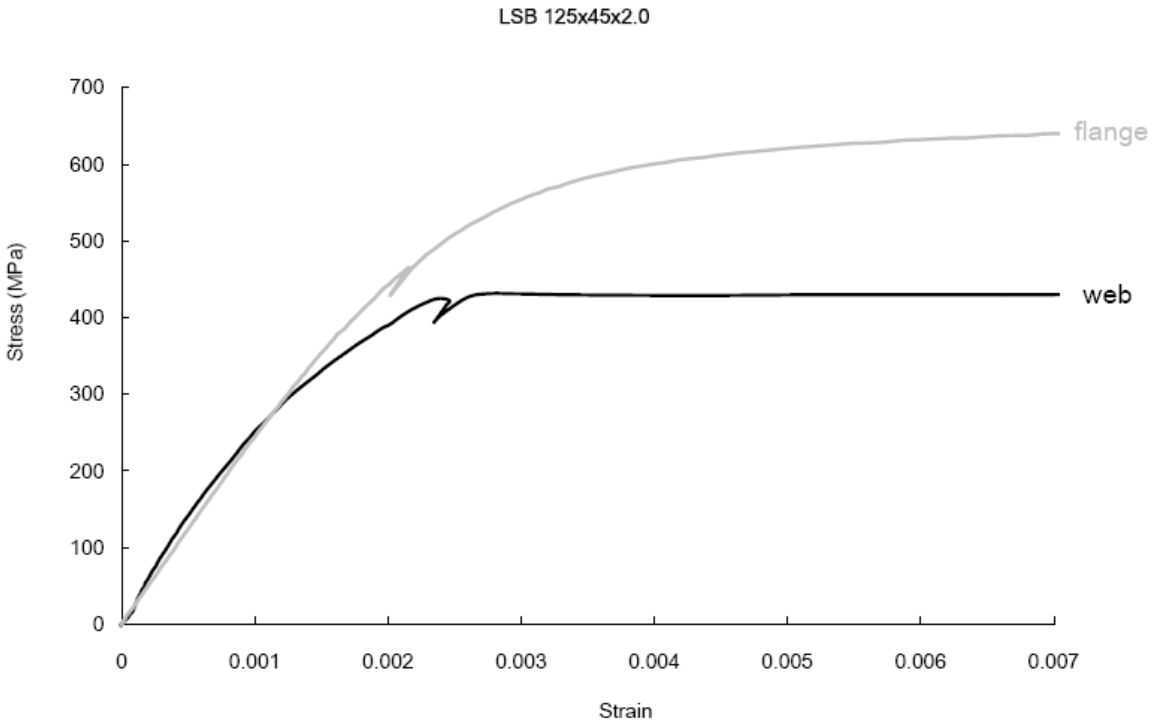

Figure 29. Stress-strain Curves of Specimen 125×45×2.0
in Web, Flange & Corner from Coupon Test

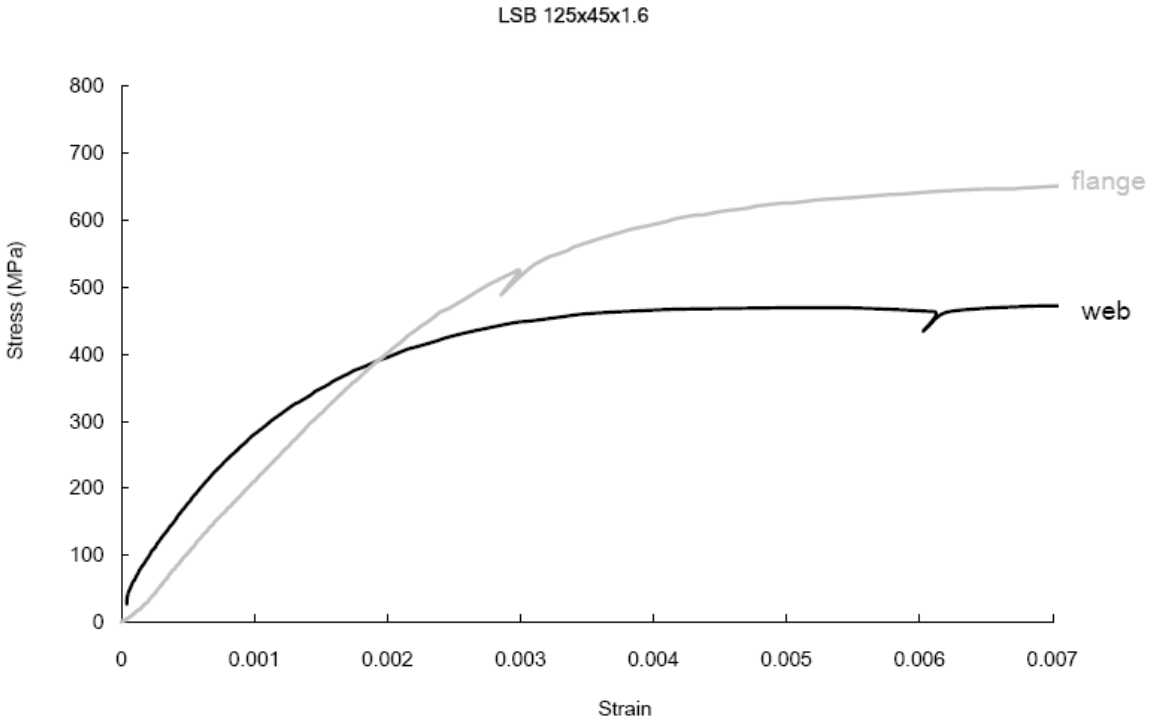

Figure 30. Stress-strain Curves of Specimen 125×45×1.6
in Web, Flange & Corner from Coupon Test

9.2 Load-displacement curves from stub column tests

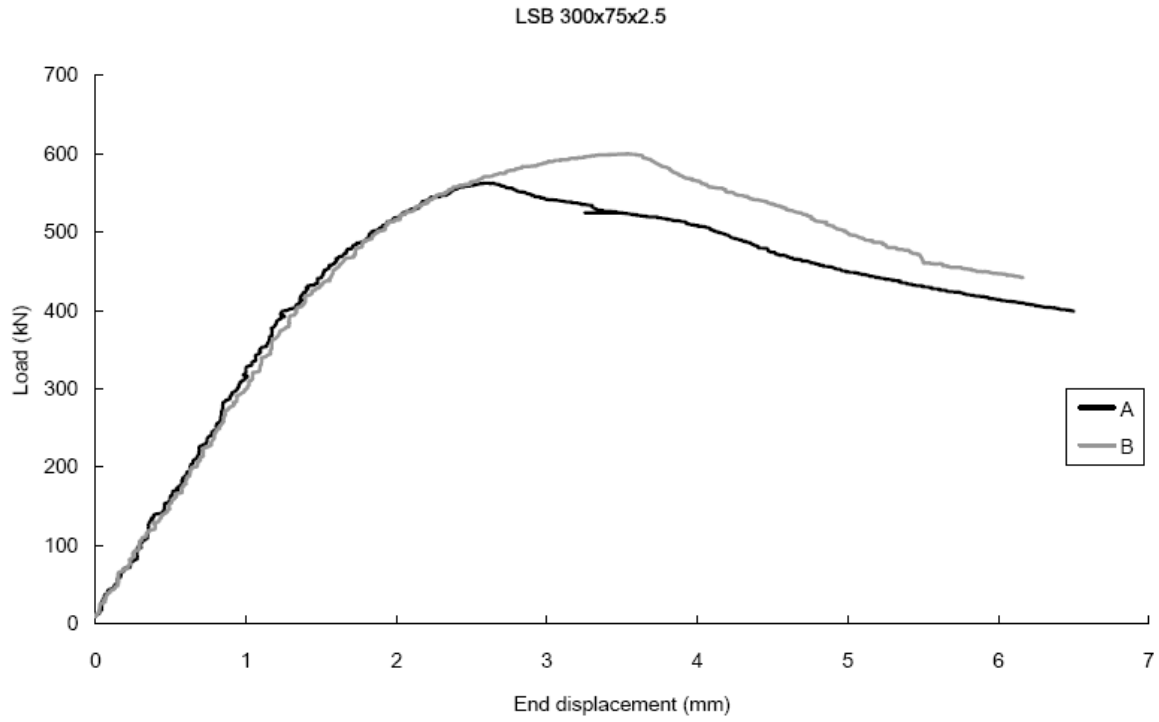

Figure 31. Load-End displacement Curves for LSB 300×75×2.5 Stub Column

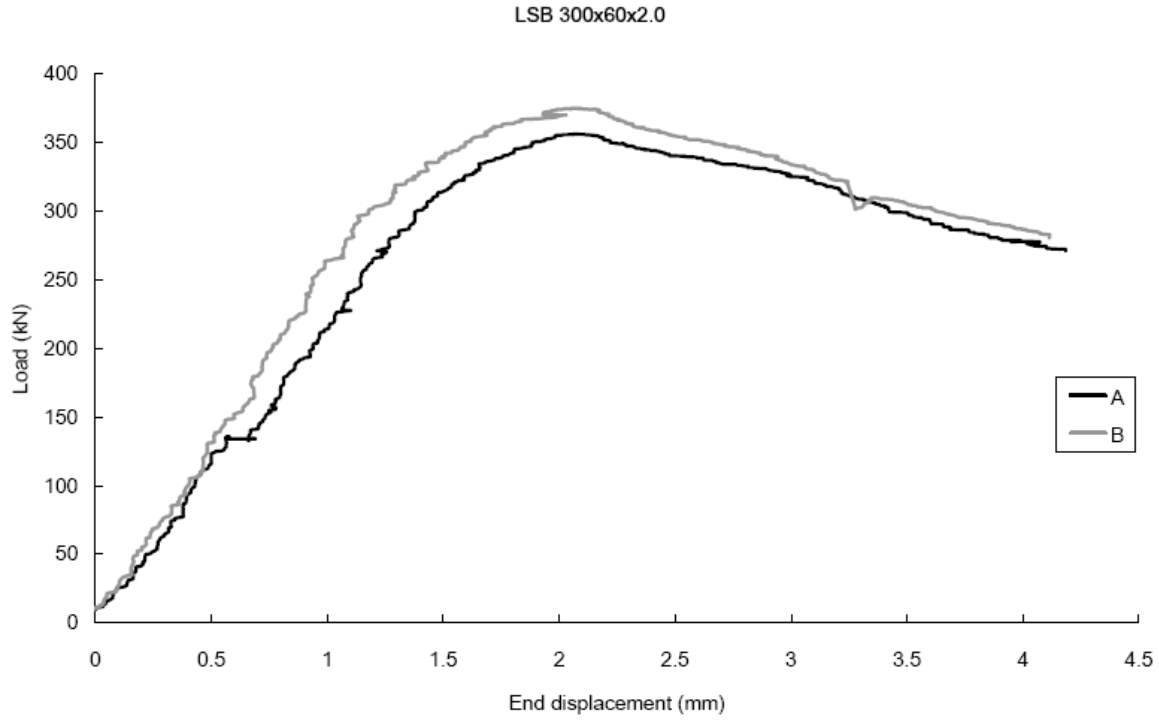

Figure 32. Load-End displacement Curves for LSB 300×60×2.0 Stub Column

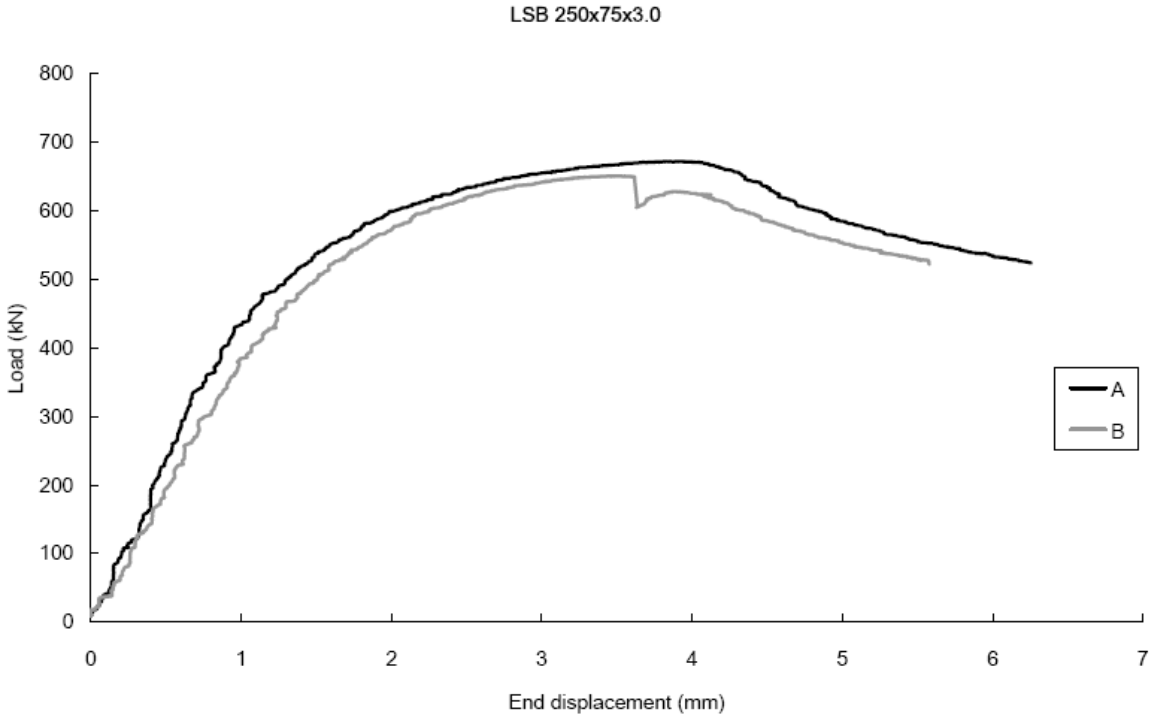

Figure 33. Load-End displacement Curves for LSB 250×75×3.0 Stub Column

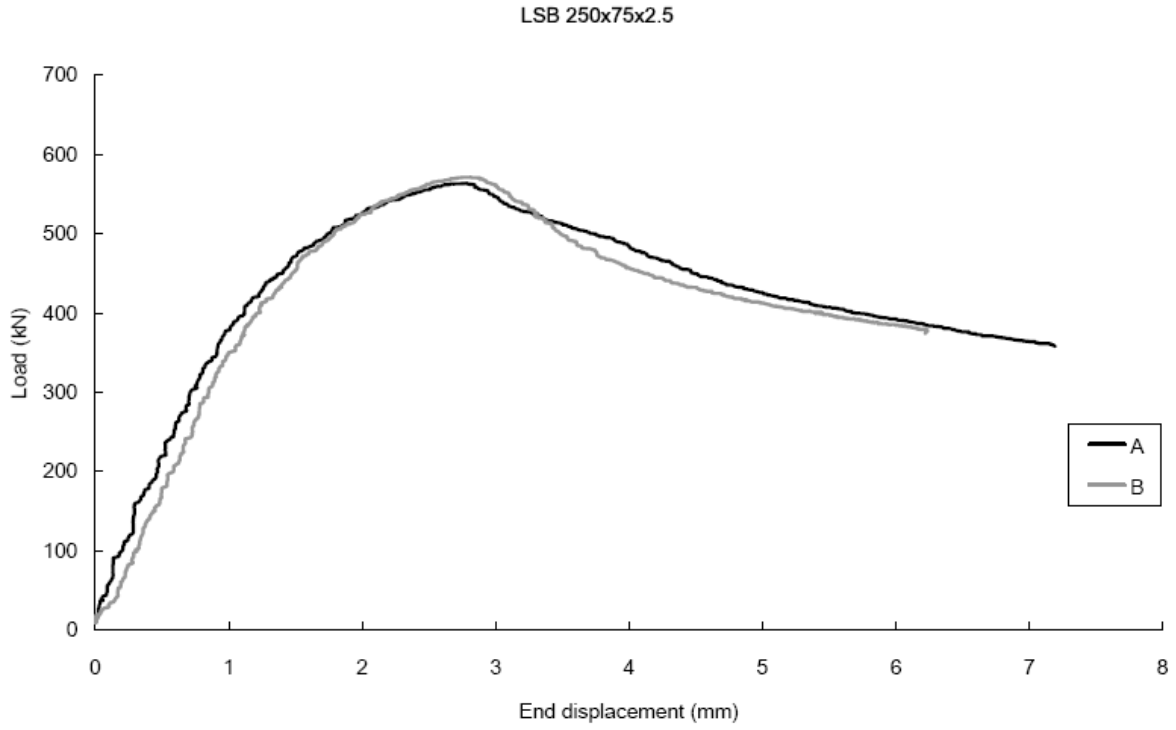

Figure 34. Load-End displacement Curves for LSB 250×75×2.5 Stub Column

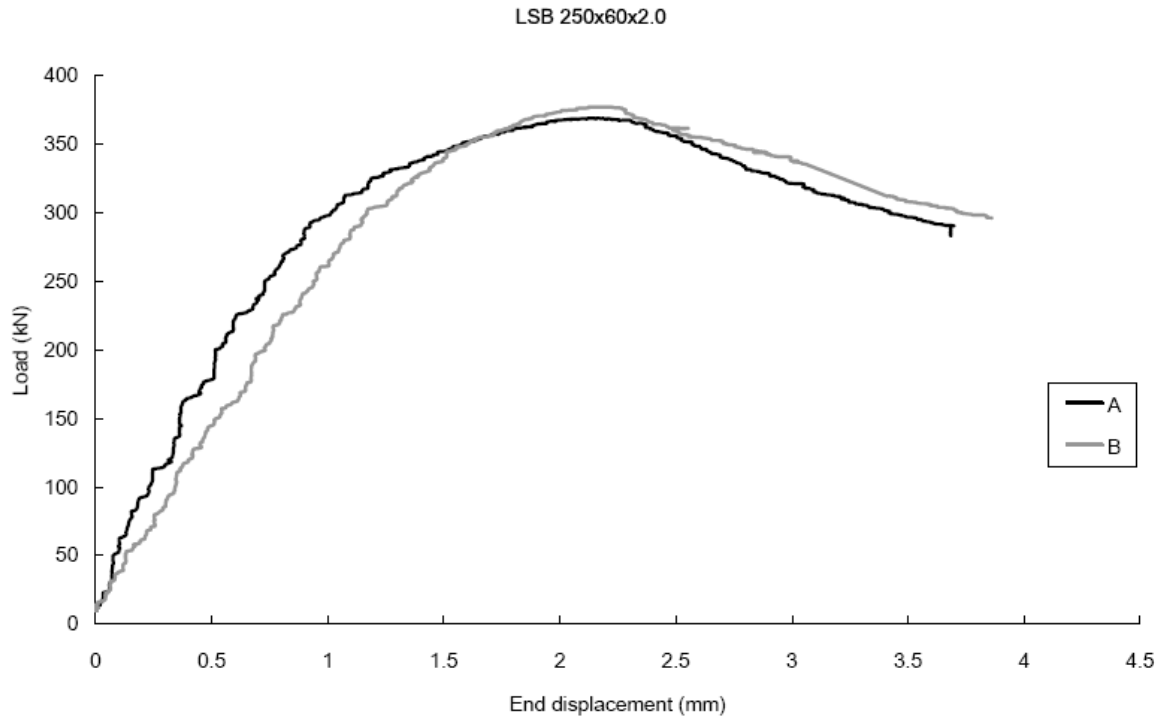

Figure 35. Load-End displacement Curves for LSB 250×60×2.0 Stub Column

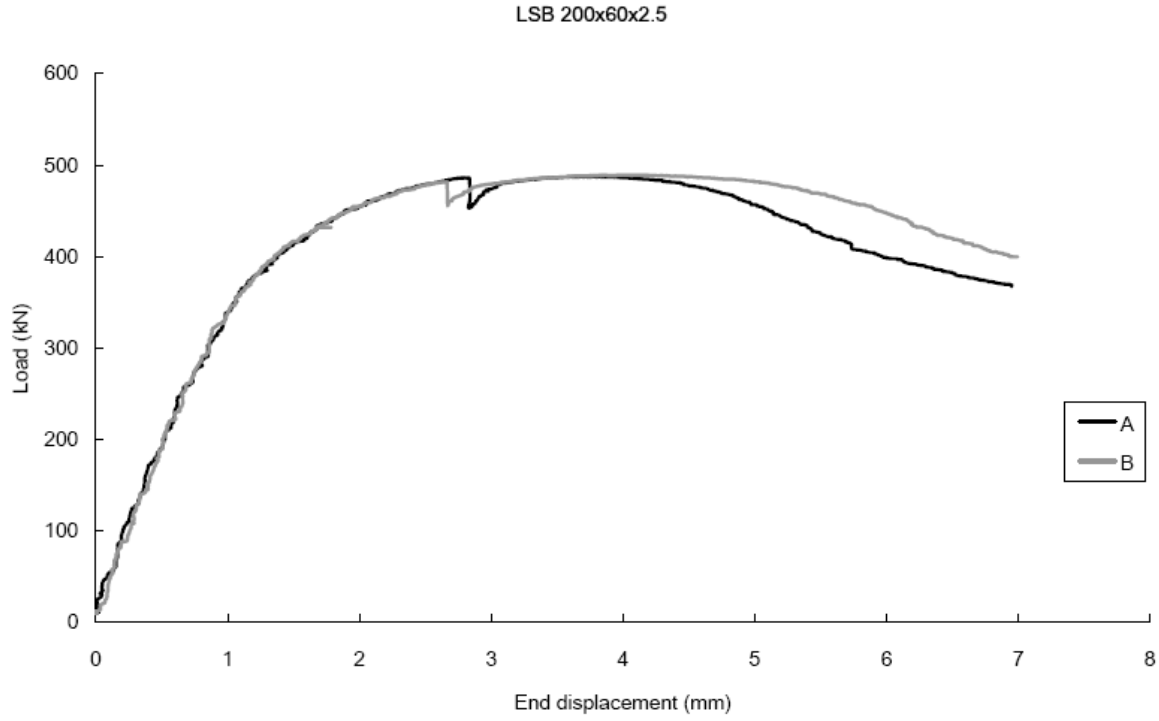

Figure 36. Load-End displacement Curves for LSB 200×60×2.5 Stub Column

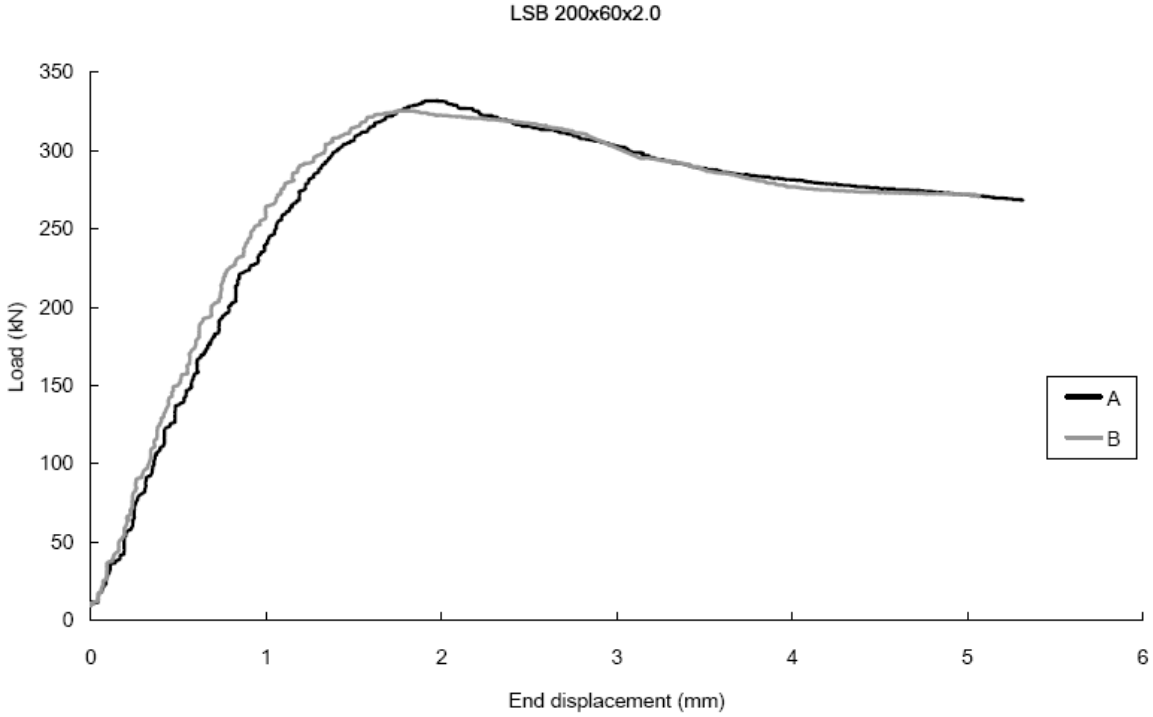

Figure 37. Load-End displacement Curves for LSB 200×60×2.0 Stub Column

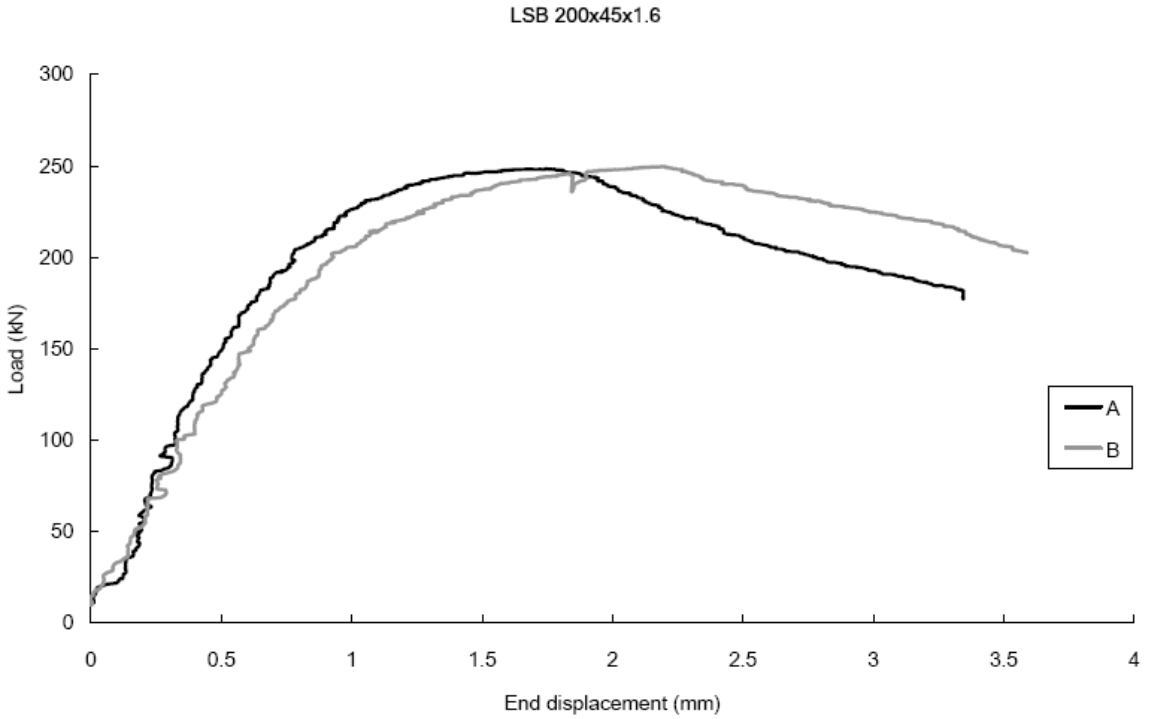

Figure 38. Load-End displacement Curves for LSB 200×45×1.6 Stub Column

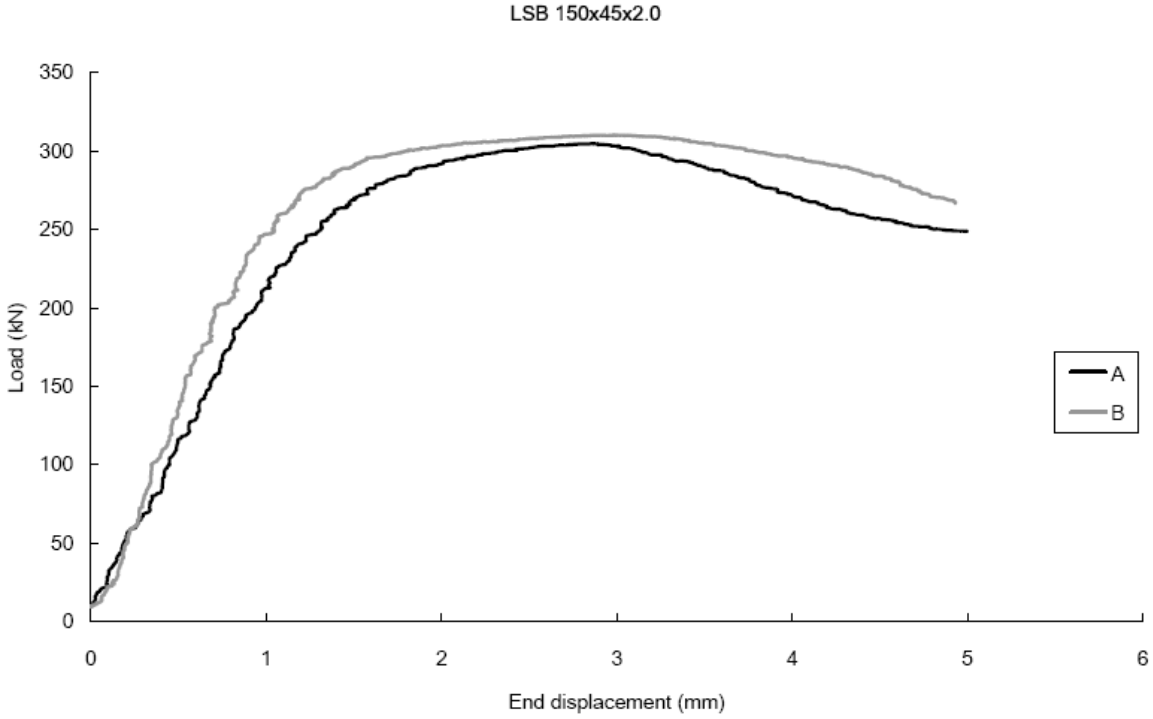

Figure 39. Load-End displacement Curves for LSB 150×45×2.0 Stub Column

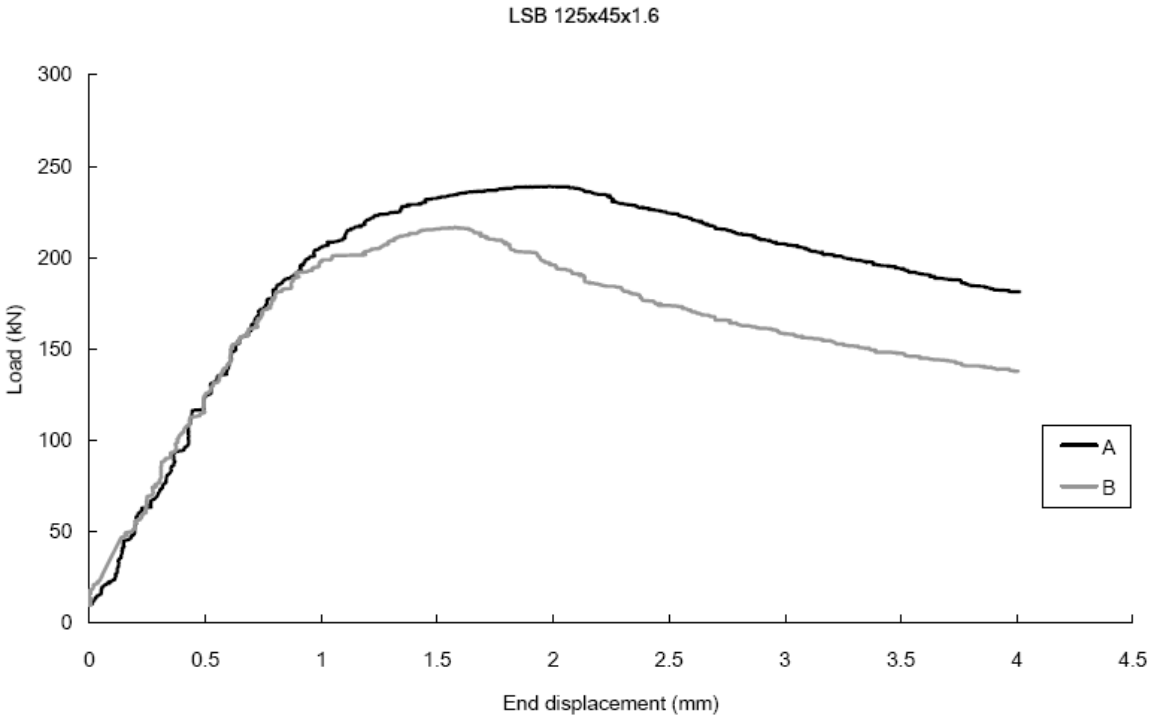

Figure 40. Load-End displacement Curves for LSB 125×45×1.6 Stub Column